

# Beyond Object Recognition: A New Benchmark towards Object Concept Learning

Yong-Lu Li Yue Xu Xinyu Xu Xiaohan Mao Yuan Yao Siqi Liu Cewu Lu\*

Shanghai Jiao Tong University

{yonglu.li, silicxuyue, xuxinyu2000, mxh1999, yaoyuan2000, magi-yunan, luewu}@sjtu.edu.cn

## Abstract

Understanding objects is a central building block of artificial intelligence, especially for embodied AI. Even though object recognition excels with deep learning, current machines struggle to learn higher-level knowledge, e.g., what attributes an object has, and what can we do with it. In this work, we propose a challenging **Object Concept Learning (OCL)** task to push the envelope of object understanding. It requires machines to reason out object affordances and simultaneously give the reason: what attributes make an object possess these affordances. To support OCL, we build a densely annotated knowledge base including extensive annotations for three levels of object concept (category, attribute, affordance), and the clear causal relations of three levels. By analyzing the causal structure of OCL, we present a baseline, **Object Concept Reasoning Network (OCRN)**. It leverages concept instantiation and causal intervention to infer the three levels. In experiments, OCRN effectively infers the object knowledge while following the causalities well. **Our data and code are available at <https://mwig-rhos.com/ocl>.**

## 1. Introduction

Object understanding is essential for intelligent robots. Recently, benefiting from deep learning and large-scale datasets [1, 2], category recognition [3, 4] has made tremendous leaps of progress. But to close the gap between human and machine perception, machines need to pursue deeper understanding, e.g., recognizing higher-level attributes [5] and affordances [6], which may help it establish object concept [7] when interacting with contexts.

Category apple is a symbol indicating its referent (real apples). In line with symbol grounding [8], machines should learn knowledge beyond category to approach concept understanding. According to cognition studies [9, 7], attribute depicting objects from the physical/visual side

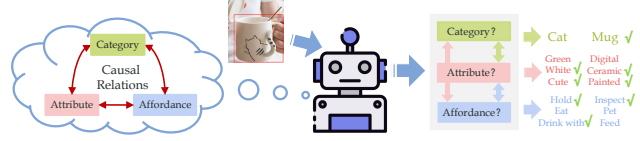


Figure 1: For embodied agents, understanding daily objects requires the ability to perceive not only **category** but also **attribute** and **affordance**. In OCL, we try to reveal object concept learning in both three levels and explore their profound causal relations.

plays an important role in object understanding. Thus, many works [10, 11, 12] studied to ground objects with attributes, e.g., a hammer consists of a long handle and a heavy head. Moreover, attributes can depict object states [5]. An elegant characteristic of attributes is *cross-category*: objects of the same category can have various states (big or fresh apple), whilst various objects can have the same state (sliced orange or apple). If the category is the **first** level of object concept, the attribute can be seen as the **second** level closer to the physical fact.

However, recognizing attributes is still far away from concept understanding. Given a hammer, we should know it can be held to hit nails, i.e., requiring machines to infer affordance [6] indicating what actions humans can perform with objects. Thus, we refer to affordance as the **third** level, which is closely related to common sense and causal inference [6]. Though affordance has been studied in robotics [13, 14] and vision [15, 16] communities for decades, it is still challenging. First, previous works [17, 18] often focus on recognizing affordance solely. But we usually infer affordance based on attribute observation. If we need to knock in a nail without a hammer at hand, we may find other hard or heavy objects instead, e.g., a thick book. This profoundly reveals the **causality** between attribute and affordance. Second, previous works are designed for scale/scene-limited tasks, e.g., in [16], 40 objects and 14 affordances are included; Hermans *et al.* [14] collect 375 indoor images of 6 objects, 21 attributes, and 7 affordances; a recent dataset [17] contains 10 indoor objects

\*Corresponding author.

and 9 affordances. Thus, they cannot afford general affordance reasoning for large-scale applications.

To reshape object learning, we believe it is essential to look at the above three levels in a **unified** and **causal** way based on an extensive knowledge base. Hence, we move a step forward to propose the object concept learning (OCL) task: given an object, machines need to infer its category, attributes, and further answer “*what can we do upon it and why*”. In a nutshell, machines need to reason affordance based on object appearance, category, and attributes. To this end, we build a large-scale and dense dataset consisting of **381** categories, **114** attributes, and **170** affordances. It contains **80,463** images of diverse scenes and **185,941** instances in different states. Different from previous works [19, 14, 16], OCL offers a more subtle angle. It includes: (1) **category-level** attribute ( $A$ ) and affordance ( $B$ ) labels; (2) **instance-level** attribute ( $\alpha$ ) and affordance ( $\beta$ ) labels. Besides, we annotate the *causal relations* between three levels to evaluate the reasoning ability of models and keep the follow-up methods from fitting data only. Accordingly, based on the causal structure of OCL, we propose a *neuro-causal* method, **Object Concept Reasoning Network (OCRN)**, as the future baseline. It leverages concept instantiation (from category-level to instance-level) and causal intervention [20] to infer attributes and affordances. OCRN outperforms a host of baselines and shows impressive performance while following the causal relations well.

In summary, our contributions are threefold: (1) Introducing the object concept learning task poses challenges and opportunities for object understanding and knowledge-based reasoning. (2) Building a benchmark consisting of diverse objects, elaborate attributes, and affordances, together with their clear causal relations. (3) An object concept reasoning network is introduced to reason three levels with concept instantiation performing well on OCL.

## 2. Related Work

**Object Attribute.** Attribute depicts the visual/physical properties like color, size, shape, etc. It usually plays the role of intermedia between pixels and higher-level concepts, *e.g.*, prompting object recognition [12], affordance learning [14], zero-shot learning [10], and object detection [21]. Recently, several large-scale datasets [12, 11, 22, 23, 5, 24, 25] are released. For attribute recognition, recent works have made progress. Besides direct attribute classification [10, 26, 11, 23] or leveraging the correlation between attribute-attribute and attribute-object [27, 28, 29], intrinsic properties (compositionality, contextuality [30, 31], symmetry [32, 33]) of attribute-object are also proven useful.

**Object Affordance.** The concept of affordance is introduced by [6]. Affordance learning has two canonical paradigms: direct mapping [18] or indirect method [16, 34,

35, 36] with intermediates like object category, attribute, and 3D contents. Some works learned affordance from human-object interaction, *i.e.*, encoding the relation between object and action [37, 38, 39]. Visual Genome [24] provides visual relations between objects, including actions instead of affordances. However, these relations cover limited and sparse affordances. Differently, we use easily accessible object images as the knowledge source, and densely annotate all attributes/affordances for all objects. Besides the vision community, the robot community pays much attention to affordance [13, 40, 41, 42], *e.g.*, for grasping and manipulation. Recently, several datasets [17, 16, 19, 15] have been proposed. Zhu *et al.* [16] built a knowledge base containing attribute, affordance, human pose, and human-object spatial configuration. But labeling pose and human-object locations are costly. Chao *et al.* [19] proposed a *semantic* category-level affordance dataset including 91 objects [2] and 957 affordances.

**Causal Inference.** There is increasing literature on exploiting causal inference [20] in machine learning, especially with causal graphical models [43, 20], including feature selection [44] and learning [45], video analysis [46, 47], reinforcement learning [48, 49], *etc.* Recently, Wang *et al.* [50] studied the causal relation between objects in images and used intervention [20] to alleviate the observation bias. Atzmon *et al.* [51] analyze the causal generative model of compositional zero-shot learning and disentangle the representations of attributes and objects. Here, we explore the causal relations between three object levels and apply backdoor adjustment [20] to alleviate the existing bias.

## 3. Knowledge Base Construction

We construct a dataset to characterize abundant object knowledge as follows (as shown in Fig. 2).

**Data Collection.** (1) **Affordance:** We collect 170 affordances out of 1,006 candidates from widely-used action/affordance datasets [19, 52, 53, 54, 16, 17] given generality and commonness. (2) **Category:** Considering the taxonomy (WordNet [55]) and diversity, we collect 381 objects out of 1,742 candidates from object datasets [12, 11, 23, 22, 2]. (3) **Attribute:** We manually filter the 500 most frequent attributes from attribute datasets [12, 11, 23, 22, 24] and choose 114 attributes, covering colors, deformations, supercategories, surface, geometrical and physical properties. (4) **Image:** We extract 75,578 images from object datasets [12, 11, 23, 22, 24], together with their Ground Truth (GT) boxes. To ensure diversity, we further manually collected 4,885 Internet images of selected categories. Then, we annotate the missing box and category labels for all instances via crowdsourcing. Finally, **185,941** instances of **381** categories from **80,463** images are collected: average of 488 instances per category and 2.31 boxes per image.

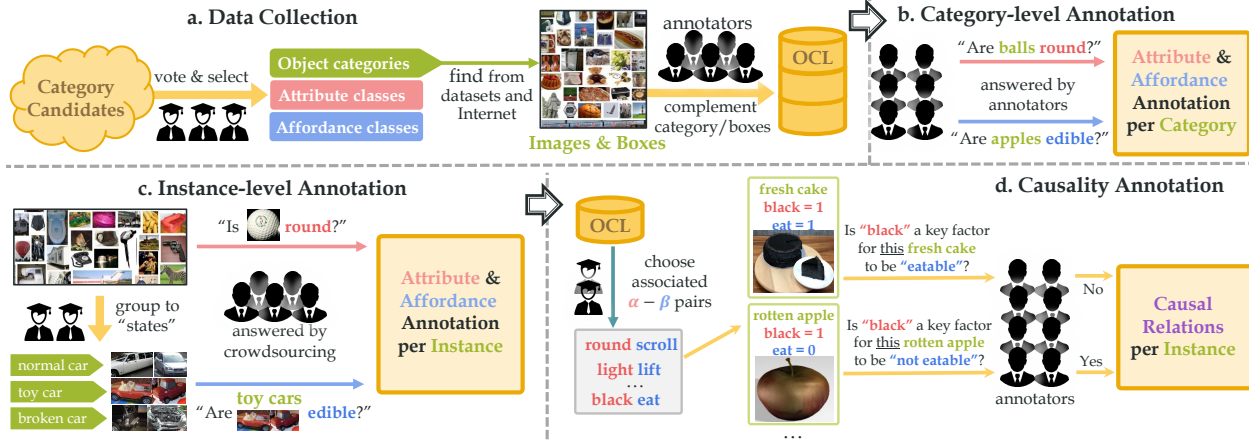


Figure 2: OCL construction. a) Data collection. b) Annotating category-level attributes and affordances. c) Annotating instance-level attributes and affordances. d) Finding direct and clear instance-level causal relations.

Details are provided in the supplementary. OCL is long-tail distributed, where the head categories have over 5,000 instances each, but the rarest categories have only 9 instances, which challenges the robustness of machines greatly.

Dataset	# Image	# Instance	# Object	# Attribute	# Affordance
APY [12]	15,339	15,339	32	64	/
SUN [11]	14,340	14,340	717	102	/
COCO-a [23]	84,044	188,426	29	196	/
ImageNet150k [22]	150,000	150,000	1,000	25	/
Chao et al. [19]	/	/	91	/	957 ( $B$ )
Hermans et al. [14]	375	-	6	21	7
Zhu et al. [16]	4,000	4,000	40	57	14
OCL	80,463	185,941	381	114	170

Table 1: Comparison of *dense annotated* datasets. OCL provides category- and instance- level attributes ( $A$ ,  $\alpha$ ), affordances ( $B$ ,  $\beta$ ).

**Annotating Attribute** in two levels of granularity: (1) **Category-level** attribute ( $A$ ) contains common sense. For each category, we annotate its *most common* attributes. In concept learning, the usage of the category-level labels as common knowledge can date back to [56]. Following [56], to avoid bias, annotators are given *category-attribute pairs* (category names instead of images) and multiple annotators vote to build the binary category-level attribute matrix  $M_A$  in size of [381, 114]. (2) **Instance-level** attribute ( $\alpha$ ) is the individual attributes of *each instance*. The annotation unit is an *attribute-instance pair*. To ensure quality, each pair is labeled by multiple annotators.

**Annotating Affordance** in two levels of granularity: (1) **Category-level** affordance  $B$ , similar to  $A$ , is annotated in *category-affordance pairs*, indicating the common affordances of each category. Following [19], the annotators label category-level affordance matrix  $M_B$  in size of [381, 170]. (2) **Instance-level** affordance  $\beta$  is annotated for *each instance* with the help of object *state*. As  $B$  is defined by common states, objects in specific states may have different affordances from  $B$ : if a service robot finds a *broken* cup, it may infer that the *cup* can still hold water as it is trained with  $B$  labels. Thus, we need detailed  $\beta$  beyond

$B$ . A state is defined as an [category, description (e.g., a set of attributes)] pair, and instances in a state usually possess similar affordances, e.g., *fresh*, *juicy*, *clean* oranges are *eatable*. First, six experts con-

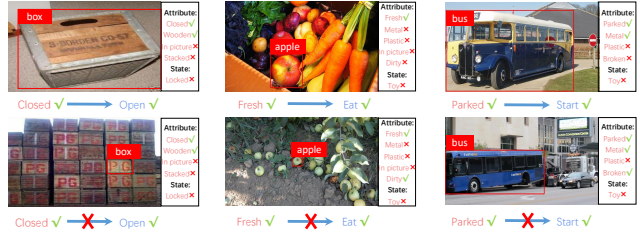


Figure 3: OCL samples including category,  $\alpha$  (red),  $\beta$  (blue), and their causal relations in various contexts. We include the states by scanning *all* instances of a category and listing all states according to affordance. Then these states were merged manually. In total, **1,376** states are defined, and each category has 3.6 states on average. Next,  $\beta$  is annotated for *each state* and the instances are first assigned with the state-level  $\beta$ . Then, the instance-level  $\beta$  is **detailed** based on the state-level  $\beta$  according to the visual content of each instance. Note that the state is category-dependent and can not be transferred among object categories, which is different from attribute and affordance. Besides, the composition of attributes makes the state space huge and there can be many *unseen* states. Thus, we only use them in annotation but not in our method.

Fig. 3 shows some examples of OCL. We compare OCL with previous dense datasets in Tab. 1. More details, figures, and tables are given in the supplementary.

## 4. Object Concept Learning

### 4.1. Causal Graph Definition

We use a causal graph to shed light on the subtle causalities of our knowledge base in Fig. 4. Causal graph [20]

indicates the underlying causalities based on components:

- $O$ : object category
- $I$ : object instance in an image
- $A, \alpha$ : category- and instance- level attributes
- $B, \beta$ : category- and instance- level affordances

According to the prior knowledge about the causalities between three levels, a hierarchical structure is depicted: (a) the **inner** triangle with dotted lines is the **category-level**: object category  $O$ , category-level attributes  $A$ , and affordances  $B$ ; (b) the **outer** triangle is the **instance-level**: instance visual appearance  $I$ , instance-level attributes  $\alpha$ , and affordances  $\beta$ . Each directed *possible* arc in the graph indicates the *possible* causality between two nodes.

Here, besides the red arcs indicating the common causal relations (e.g.,  $I \rightarrow \alpha$ ,  $I \rightarrow \beta$  as attribute/affordance recognition from images), we also define some special arcs given our category-level attribute and affordance settings: (1)  $O \rightarrow A$ ,  $O \rightarrow B$  (dotted arcs): Given  $O$ ,  $A, B$  are strictly *determined* within labels. (2)  $O \rightarrow I$ ,  $A \rightarrow \alpha$ ,  $B \rightarrow \beta$  (blue arcs): The category-level  $O$ ,  $A$ , and  $B$  are direct causes of instance-level  $I$ ,  $\alpha$ , and  $\beta$  during the concept *instantiation*. Note that, according to the previous analysis, we focus on the  $A \rightarrow B$  and  $\alpha \rightarrow \beta$  but sometimes the opposite can also happen:  $A \leftarrow B$  and  $\alpha \leftarrow \beta$ . Thus, we also draw them in Fig. 4. We will analyze them later.

In this work, we focus on  $\alpha, \beta$  perception ( $I \rightarrow \alpha$ ,  $I \rightarrow \beta$ ) and visual reasoning (with  $I$ , inferring  $\beta$  given  $\alpha$ ) for embodied AI. Thus, Fig. 4 is a simplified causal graph. Our knowledge base can support more tasks such as attribute/affordance conditioned image generation ( $\alpha \rightarrow I$ ,  $\beta \rightarrow I$ ) [57]. However, they are beyond the scope of this paper. In the supplementary, we give more discussions.

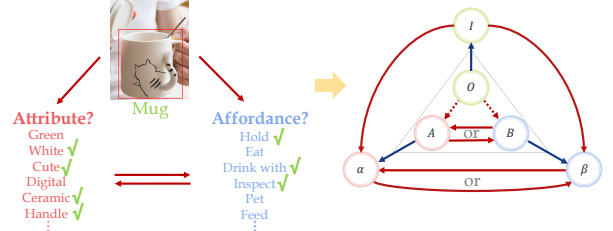
## 4.2. Task Overview

Given an instance  $I$  (content in box  $b_o$  representing an object instance), the OCL task aims to infer attribute  $\alpha$  and affordance  $\beta$  while following the causalities. Formally, OCL can be described as:

$$\langle P_\alpha, P_\beta \rangle = \mathcal{F}(I, P(O|I)), \quad (1)$$

where  $P_\alpha, P_\beta$  are the probabilities of  $\alpha, \beta$ ,  $P(O|I)$  is the predicted category probability from an object detector [4].

We aim at benchmarking the reasoning ability of machines, causal relations in Fig. 4 can all be candidates. However, after some user studies on annotating different arcs, we find that annotating causal relations is usually ambiguous and impractical to cover all relations. Moreover, from the aspect of embodied AI, affordance  $\beta$  is more important in the interactions between robots and the physical world. Thus, we mainly measure the learning of  $\alpha \rightarrow \beta$  and only annotate the unambiguous  $\alpha \rightarrow \beta$  in OCL (Sec. 4.3). Moreover, both the causal relation annotation process and the ablations in Sec. 5 support that the causal effect of  $\alpha \rightarrow \beta$  is



(a) OCL: Object Concept Learning (b) Causal Graph  
Figure 4: Causal graph of our OCL task. “or” indicates that either  $A \leftarrow B$  or  $A \rightarrow B$  ( $\alpha \rightarrow \beta$  or  $\alpha \leftarrow \beta$ ) exists.

more significant than the other alternatives. In the following tasks, we focus more on  $\beta$  and the arc  $\alpha \rightarrow \beta$ . Formally, the evaluation of  $\alpha \rightarrow \beta$  learning follows

$$\Delta P_\beta = ITE[\mathcal{F}(I, P(O|I))], \quad (2)$$

where  $\Delta P_\beta$  is the Individual Treatment Effect [58] of **affordance prediction change** after we operate  $ITE[\cdot]$  on a model  $\mathcal{F}(\cdot)$ .  $\Delta P_\beta$  is expected to follow the GT causal relation between  $\alpha, \beta$  from humans. For example, when the attributes of an object change, then the causal-related affordances should also change accordingly. We will introduce the ITE evaluation in Sec. 5. Note that though there is an arc from  $A$  to  $B$ ,  $A, B$  are decided by  $O$ . Given  $O$ , we can get  $A, B$  via querying the prior  $M_A, M_B$  (Sec. 3). Thus, we do not evaluate this arc here.

We split images into the train, validation, and test sets with 56K:14K:9K images. The validation and test sets cover 221 of the 381 categories, and the train set covers all categories. OCL is a long-tailed recognition task [59, 60] and requires generalization to cover the whole object category-attribute-affordance space with imbalanced information. Thus, it is challenging for current vision systems without the reasoning ability to understand the causalities.

## 4.3. Benchmarking Causal Inference on $\alpha \rightarrow \beta$

We annotate *instance-level* (considering the context of each instance) causality of  $\alpha \rightarrow \beta$  to answer *which attribute(s) are the critical and direct causes of a certain affordance?* in two phrases:

**Filtering** to avoid the combinatorial explosion. Initially, we need to make binary decisions on all *instance- $\alpha$ - $\beta$*  triplets, which is far beyond handleable. Fortunately, we find that **most**  $\alpha$ - $\beta$  classes (e.g., shiny and kick) are meaningless and always of no causality in any instances. Thus, we can first exclude the most impossible pairs, meanwhile, guarantee the completeness of causality. Finally, we obtain about 10%  $\alpha$ - $\beta$  classes as candidates.

**Instance-level Causality:** we adopt object states as a reference. Multiple annotators have been involved for each *state- $\alpha$ - $\beta$*  triplet and are asked whether the specific attribute is the *clear* and *direct* cause of this affordance in this state. The answers are combined and checked for all instances of



a state. Finally, we obtain about 2 M *instance- $\alpha$ - $\beta$*  triplets of causal relations. As we have labeled all  $\alpha$  and  $\beta$  for all instances, the causal relations would be in four situations: [0,0], [1,1]; [0,1], [1,0]. The former two are “positive”, *e.g.*, *fresh*(1/0)→*eat*(1/0) for an *apple*. While the last two are “negative”, *e.g.*, *broken*(1/0)→*drive*(0/1) for a *car*.

Fig. 3 shows some causal examples. These causalities are not thoroughly studied in previous datasets [16, 17, 18, 14]. For more details, please refer to the supplementary.

#### 4.4. Object Concept Reasoning Network

Before proposing our method, we first simplify the causal graph in Fig. 4 to facilitate the graph implementation of the proposed OCRN. First, we focus on the more significant  $\alpha \rightarrow \beta$  and omit  $\beta \rightarrow \alpha$ . Similarly, we omit  $B \rightarrow A$ . Moreover,  $I, \alpha, \beta$  are the *instantiations* of  $O, A, B$  respectively and we use a whole node  $O'$  to represent  $O, A, B$ . Thus, the adopted causal graph is shown in Fig. 5.

Our OCRN implements the **instantiation** of attribute and affordance, corresponding to the arcs  $A \rightarrow \alpha, B \rightarrow \beta$ . Thus the model can propose a coarse estimation of attribute and affordance at category-level, then tune the results with the visual patterns of the image as a condition for a more accurate prediction. Besides, we also exploit **intervention** to remove the causal relation between  $I$  and  $O$  to construct a category-agnostic model. It suffers less from category bias and is more capable of learning uncommon cases.

**Object Category Bias.** Formally, OCL is depicted as  $P(\alpha|I)$  and  $P(\beta|I, \alpha)$ . As the samples of different object categories are usually imbalanced, conventional methods may suffer from severe *category bias* [50]. For example, in OCL, animal accounts for 22% instances, and home appliance only accounts for 3%. In  $P(\alpha|I)$ , category bias is imported following

$$P(\alpha|I) = \sum_i^m P(\alpha|I, O_i)P(O_i|I), \quad (3)$$

where  $P(O_i|I)$  is the predicted category probability. That is,  $O$  is a confounder [20] and pollutes attribute inference, especially for the *rare* categories.

**Causal Intervention.** To tackle this, we propose OCRN using intervention [20] to deconfound the confounder  $O$  for  $\alpha$  (Fig. 5). In  $\alpha$  estimation, we use  $do(\cdot)$  operation [20] to eliminate the arc from  $O$  to  $I$ :  $P(\alpha|do(I))$  is

$$\begin{aligned} & \sum_i^m P(\alpha|I, O_i)P(O_i) \\ &= \sum_i^m P(O_i) \sum_j^m P(\alpha|I, A_j)P(A_j|O_i) \\ &= \sum_i^m P(\alpha|I, A_i)P(O_i), \end{aligned} \quad (4)$$

where  $m = 381$ .  $A_j$  is the category-attribute vector of  $j^{th}$  category. As  $A$  is decided by  $O$ ,  $P(A_j|O_i) = 1$  if  $i = j$  and  $P(A_j|O_i) = 0$  if  $i \neq j$ , where  $O_i$  is the  $i^{th}$  category and  $A_j$  is the category-attribute of  $j^{th}$  category.  $P(O_i)$  is the **prior** probability of the  $i$ -th category (frequency in our train set). We apply the intervention to reduce the bias from  $O$  recognition for an **category-agnostic** model.

Similar to  $\alpha$ , in  $\beta$  estimation, category bias also exists:

$$P(\beta|I, \alpha) = \sum_i^m P(\beta|I, \alpha, O_i)P(O_i|I, \alpha). \quad (5)$$

With Eq. 4,  $\alpha$  can be seen as “enforced” and deconfounded, as it is beforehand estimated. For  $I$ , we again use intervention [20]:

$$P(\beta|do(I, \alpha)) = \sum_i^m P(\beta|I, \alpha, B_i)P(O_i). \quad (6)$$

Similar to Eq. 4,  $P(B_j|O_i) = 1$  if  $i = j$ ,  $P(B_j|O_i) = 0$  if  $i \neq j$ , we omit the process for clarity.

##### 4.4.1 Model Implementation

We represent nodes  $\{I, A, B, \alpha, \beta\}$  as  $\{f_I, f_A, f_B, f_\alpha, f_\beta\}$  respectively in latent space.  $f_I$  is the RoI pooling feature of an instance extracted by a COCO pre-trained ResNet-50 [61]. Following Eq. 4, we represent category-level attribute  $A$  based on the *mean* object category feature  $\bar{f}_{O_i}$ , which is the mean of  $f_I$  of all **training** samples in category  $O_i$ . We map  $\bar{f}_{O_i}$  to the attribute latent space  $f_{A_i}$  with fully-connected layers (FC) (Fig. 5).  $f_{A_i}$  stands for the category-attribute representation for  $i^{th}$  category.

**Attribute Instantiation.** Next, we obtain  $\alpha$  representation following Eq. 4:

$$f_{\alpha_i} = \mathcal{F}_\alpha(f_I, f_{A_i}), \quad f_\alpha = \sum_i^m f_{\alpha_i} \cdot P_{O_i}, \quad (7)$$

where  $P_{O_i}$  is the *prior* category probability ( $P(O_i)$  in Eq. 4). Eq. 7 indicates the attribute *instantiation* from  $A$  to  $\alpha$  with  $I$  as the *condition*. Hence, we can equally translate the  $\alpha$  estimation problem into a **conditioned instantiation problem**.  $\mathcal{F}_\alpha(\cdot)$  is implemented with multi-head attention [62] with two entries (Fig. 5). The attention output is compressed by a linear layer to the instantiated representation  $f_{\alpha_i}$ . The debiased representation  $f_\alpha$  is the expectation of  $f_{\alpha_i}$  w.r.t  $P_{O_i}$  according to back-door adjustment in Eq. 4.

We also get the feature for specific attributes for ITE operation in Sec. 5.  $f_\alpha$  is first separated to  $f_{\alpha_p}$  for each attribute  $p$  ( $p \in [1, 114]$ ) by multiple independent FCs, then we can manipulate specific attributes by masking some certain  $f_{\alpha_p}$ . Next, the features are further aggregated via

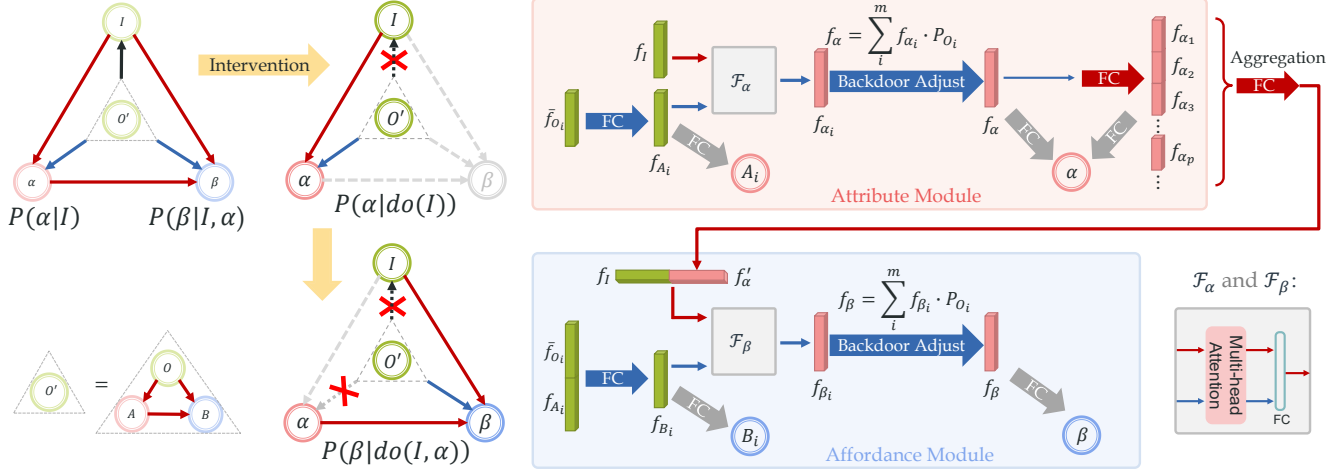


Figure 5: The overview of OCRN. The arc from  $O$  to  $I$  is deconfounded. Thus we can eliminate the bias from the  $O$  imbalance. Equations below the graphs are the original or deconfounded estimations of  $\alpha, \beta$ . Attribute and affordance modules are the **instantiations** of category-level features: categorical representations  $f_{A_i}$  or  $f_{B_i}$  are obtained following the left-bottom-most causal graph, and then instantiated via  $\mathcal{F}_\alpha$  or  $\mathcal{F}_\beta$  conditioned by the instance representations.  $f_\alpha$  and  $f_\beta$  after intervention are the expectations of instantiated  $f_{\alpha_i}$  and  $f_{\beta_i}$  w.r.t **prior**  $P_{O_i}$ . At last, linear-Sigmoid classifiers give the final predictions.

concatenating-compressing by an FC to  $f'_\alpha$  as shown in Fig. 5.

**Affordance Instantiation.** Similarly, FCs are used to obtain  $f_\beta$  from  $f_{O_i}$  and  $f_{A_i}$  and Eq. 6 is implemented as:

$$f_{\beta_i} = \mathcal{F}_\beta(f_I, f'_\alpha, f_{B_i}), \quad f_\beta = \sum_i^m f_{\beta_i} \cdot P_{O_i}. \quad (8)$$

Given the conditions  $\{f_I, f'_\alpha, f_{B_i}\}$ ,  $\mathcal{F}_\beta(\cdot)$  operate the instantiation.

#### 4.4.2 Learning Objectives.

To drive the learning, we devise several objectives:

**Category-level loss  $L_C$ .** We input category-level  $f_A, f_B$  to two linear-Sigmoid classifiers to classify  $A, B$ . The binary cross-entropy losses are  $L_A$  and  $L_B$ . The total category-level loss is  $L_C = L_A + L_B$ .

**Instance-level loss  $L_I$ .** We input instance-level  $f_\alpha, f_\beta$ , together with  $f_{\alpha_i}, f_{\beta_i}$  to linear-Sigmoid classifiers. The separated  $f_{\alpha_p}$  are also sent to independent binary classifiers. The binary cross-entropy losses are represented as  $L_\alpha, L_\beta$ . The total instance-level loss is  $L_I = L_\alpha + L_\beta$ .

The total loss is  $L = \lambda_C L_C + L_I$ . We adopt a two-stage policy: first inferring attributes, then reasoning affordances.

## 5. Experiment

**Metric.** We design different metrics for the recognition and reasoning tasks:

$\alpha, \beta$  **Recognition:** we measure the correctness of model prediction  $\hat{\alpha}$  and  $\hat{\beta}$ . For multi-label classification tasks, we use the mean Average Precision (mAP) metric.

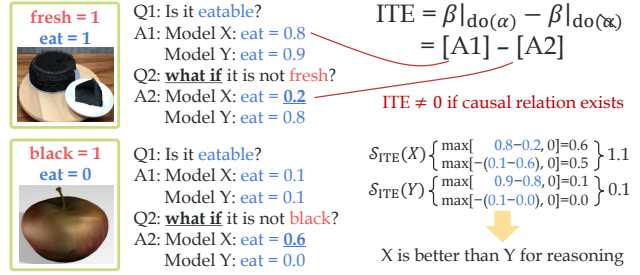


Figure 6: Example of ITE reasoning benchmark.

**Reasoning:** we use **Individual Treatment Effect (ITE)** [58].  $ITE_i = Y_{i,T=1} - Y_{i,T=0}$  measures the causal effect  $T \rightarrow Y$  of  $i^{\text{th}}$  individual with the difference between outcomes ( $Y$ ) with or without receiving the treatment ( $T$ ). In OCL, we discuss the causal relation between  $p^{\text{th}}$  attribute and  $q^{\text{th}}$  affordance:  $\alpha_p \rightarrow \beta_q$ . So we interpret the treatment  $T$  as the **existence of  $\alpha_q$**  and the outcome  $Y$  as the  $\beta_q$  output. We measure the difference of  $\beta_q$  output when the whole  $\alpha_q$  feature is wiped out or not, which should be non-zero when the causal relation  $\alpha_p \rightarrow \beta_q$  exists.

In detail, given an OCL model, for an instance with causal relation  $\alpha_p \rightarrow \beta_q$  ( $p \in [1, 114], q \in [1, 170]$ ), we first formulate ITE as the **affordance probability change** following Eq. 2:

$$ITE = \Delta \hat{\beta}_q = \hat{\beta}_q|_{do(\alpha_p)} - \hat{\beta}_q|_{do(\alpha_{\emptyset})}, \quad (9)$$

where  $\hat{\beta}_q|_{do(\alpha_p)}$  is the factual output of the affordance probability of the model.  $\hat{\beta}_q|_{do(\alpha_{\emptyset})}$  is the counterfactual output when the  $\alpha_p$  is wiped out, which can be obtained by assign zero-mask [63] to the feature of  $\alpha_p$  (e.g.,  $f_{\alpha_p}$  in OCRN) and keep the other features.

Then, based on ITE, we benchmark instances following:

**ITE:** If the causality  $\alpha_p \rightarrow \beta_q$  exists on the instance, ITE should be non-zero when eliminating the effect of  $\alpha_p$ . And the direction of ITE depends on the affordance ground-truth  $\beta_q$ : if  $\beta_q = 0$ , the predicted  $\hat{\beta}_q$  tend to be 1 after wiping out  $\alpha_p$  so ITE should be a negative value; contrarily, ITE should be positive if  $\beta_q = 1$ . Hence we compute the ITE score as:

$$\mathcal{S}_{\text{ITE}} = \begin{cases} \max(\Delta\hat{\beta}_q, 0), & \beta_q = 1, \\ \max(-\Delta\hat{\beta}_q, 0), & \beta_q = 0, \end{cases} \quad (10)$$

so that larger  $\mathcal{S}_{\text{ITE}}$  score indicates the model infers more accurate ITE directions and has better reasoning performance.

**$\alpha$ - $\beta$ -ITE:** we combine recognition and reasoning performances. We multiply  $\mathcal{S}_{\text{ITE}}$  with  $P(\hat{\alpha}_p = \alpha_p)$  and  $P(\hat{\beta}_q = \beta_q)$  as a unified metric  $\mathcal{S}_{\alpha-\beta\text{-ITE}}$ .

For both metrics, we compute AP for each  $[\alpha_p, \beta_q]$  and average them to mAP.

**Baselines.** Different methods exploit different causal paths including the sub-graphs with  $\alpha \rightarrow \beta$  or  $\alpha \leftarrow \beta$  based on Fig. 4. We implement 14 baselines following different sub-graphs to fully exert the potential of OCL and divide them into 3 folds w.r.t.  $\alpha - \beta$  causal structure. We briefly list them here and detail them in the supplementary:

**Fold I.** No arc connecting  $\alpha$  and  $\beta$ :

(1) Direct Mapping from  $f_I$  to  $P_\alpha, P_\beta$  via an MLP (DM-V): feeding  $f_I$  into MLP-Sigmoids to predict  $P_\alpha, P_\beta$ .

(2) DM Linguistic feature (DM-L): replacing the  $f_I$  of DM-V with linguistic feature  $f_L$ , which is the expectation of Bert [64] embeddings of category names w.r.t  $P(O_i|I)$ .

(3) Visual-Linguistic alignment, *i.e.*, Multi-Modality (MM): mapping  $f_I$  to a latent space and minimizing the distance to  $f_L$ , then feeding it to an MLP-Sigmoids to predict  $\alpha, \beta$ .

(4) Linguistic Correlation of  $O$ - $\alpha$ ,  $O$ - $\beta$  (LingCorr): measuring the correlation between object and  $\alpha$  or  $\beta$  classes via their Bert [64] embedding cosine similarities.  $P_\alpha, P_\beta$  are given by multiplying  $P(O|I)$  to correlation matrices.

(5) Kernelized Probabilistic Matrix Factorization (KPMF) [65]: calculating feature similarity to all training samples as weights. Taking the weighted sum of GT  $\alpha$  or  $\beta$  of training samples as predictions.

(6) A&B Lookup: getting  $P_A, P_B$  from  $M_A, M_B$ .

(7) Hierarchical Mapping (HMa): mapping  $f_I$  to category-level attribute or affordance space by an MLP, then feeding it to an MLP-Sigmoids to predict  $P_\alpha$  or  $P_\beta$ .

**Fold II.**  $\beta \rightarrow \alpha$ :

(8) DM from  $\beta$  to  $\alpha$  (DM- $\beta \rightarrow \alpha$ ): same as DM-V but using  $f_\beta$  to infer  $\alpha$ .

(9) DM from  $\beta$  and  $I$  to  $\alpha$  (DM- $\beta I \rightarrow \alpha$ ): same as DM-V but using both  $f_I$  and  $f_\beta$  to infer  $\alpha$ .

**Fold III.**  $\alpha \rightarrow \beta$ :

(10) DM from  $\alpha$  to  $\beta$  (DM- $\alpha \rightarrow \beta$ ): same as DM-V but using both  $f_I$  and  $f_\alpha$  to infer  $\beta$ .

(11) DM from  $\alpha$  and  $I$  to  $\beta$  (DM- $\alpha I \rightarrow \beta$ ): same as DM-V but using both  $f_I$  and  $f_\alpha$  to infer  $\beta$ .

(12) Retrieving  $\alpha$ - $\beta$  relation by Ngram [66] (Ngram): adopting Ngram to retrieve the relevance of  $\alpha$  &  $\beta$ . Then we use DM predicted  $\alpha$  and the relevance to estimate  $\beta$ .

(13) Markov Logic Network [67] (MLN-GT): using GT  $\alpha$  to infer  $\beta$  with MLN.

(14) Instantiation with attention (Attention): feeding  $[f_\alpha, f_I]$  to an MLP-Sigmoid to generate attentions and predicting  $P_\beta$  by multiplying the attentions with  $P_B$ .

**ITE loss.** Though machines are expected to learn the causalities given  $\alpha, \beta$  labels only. We wonder how it would perform given *causal supervision*. We adopt an extra Hinge loss to maximize the ITE score of all  $[\alpha_p, \beta_q]$ . In detail, we intend the ITE of causal relations larger than a margin  $\tau$  ( $= 0.1$  in experiments), so the loss term is:

$$\begin{cases} \max\{0, \tau - \Delta\hat{\beta}_q\}, & \beta_q = 1, \\ \max\{0, \tau + \Delta\hat{\beta}_q\}, & \beta_q = 0. \end{cases} \quad (11)$$

We enumerate all *annotated*  $[\alpha_p, \beta_q]$  of an instance to obtain  $L_{\text{ITE}}$ . Different from the default, the total loss here is  $L = \lambda_C L_C + L_I + \lambda_{\text{ITE}} L_{\text{ITE}}$ .

**Implementation Details.** For a fair comparison, all methods adopt a shared COCO [2] pre-trained ResNet-50 [61] (frozen) to extract  $f_I$  and use the same object boxes in training and inference. In OCRN, the dimension of  $f_I$  and all  $f_{A_i}, f_{B_i}, f_\alpha, f_\beta$  is 1024. The individual features of each attribute category are 512d and aggregated to 1024d by an FC. We train the attribute module with a learning rate of 0.3 and batch size of 1024 for 470 epochs. Then the attribute module is frozen, and the affordance module is trained with a learning rate of 3.0e-3 and batch size of 768 for 20 epochs. In training,  $\lambda_C = 0.03$ ,  $\lambda_{\text{ITE}} = 3$ .

**Results.** Tab. 2 presents the results. We can find that the causal structure of the models matters in OCL. Comparing DM methods implementing different causal graphs (including  $\alpha \rightarrow \beta$ ,  $\alpha \leftarrow \beta$ ),  $\alpha$  as intermediate knowledge (DM- $\alpha \rightarrow \beta$  and DM- $\alpha I \rightarrow \beta$ ) could advance  $\beta$  perception (DM-V). But when  $\beta$  serves as intermediate (DM- $\beta \rightarrow \alpha$  and DM- $\beta I \rightarrow \alpha$ ),  $\beta$  perception is comparable or even worse than DM-V. So the causal relation  $\alpha \rightarrow \beta$  is more evident than  $\beta \rightarrow \alpha$  in the realistic dataset, which supports our choice in Sec. 4.2 that we focus more on the  $\alpha \rightarrow \beta$  arc and implement our model with only  $\alpha \rightarrow \beta$ .

OCRN outperforms the baselines and achieves decent improvements on all tracks. In terms of  $\alpha$  recognition, with or without  $L_{\text{ITE}}$ , OCRN outperforms the second-best method with 1.7 and 2.5 mAP respectively. As for  $\beta$  recognition, the improvements are 0.7 and 1.1 mAP with or without  $L_{\text{ITE}}$ . Comparatively, HMa utilizes the supervision of  $A, B$ , but it performs much worse. A&B Lookup directly uses GT  $A, B$  to infer  $\alpha, \beta$ , but its poor performance verifies

Fold	Method	$\alpha$	$\beta$	$\mathcal{S}_{ITE}$	$\mathcal{S}_{\alpha-\beta-ITE}$
i N/A	DM-V	29.9	51.8	-	-
	DM-L	21.2	47.5	-	-
	MM	23.8	48.9	-	-
	LingCorr	7.9	25.9	-	-
	KPMF	25.4	49.1	-	-
	A&B-Lookup	18.9	30.9	-	-
	HMa	28.6	51.7	-	-
ii: $\beta \rightarrow \alpha$	DM- $\beta \rightarrow \alpha$	30.0	52.0	-	-
	DM- $\beta I \rightarrow \alpha$	29.5	51.8	-	-
iii: $\alpha \rightarrow \beta$	DM- $\alpha \rightarrow \beta$	28.7	52.6	7.6	6.7
	DM- $\alpha I \rightarrow \beta$	29.0	52.6	8.1	7.0
	Ngram	22.6	50.8	8.3	7.6
	MLN-GT	-	33.4	9.5	9.1
	Attention	24.1	48.9	8.1	7.1
	OCRN	31.6	53.3	9.5	9.2
$\alpha \rightarrow \beta$	DM- $\alpha \rightarrow \beta$ w/ $L_{ITE}$	28.8	52.4	15.5	14.0
	DM- $\alpha I \rightarrow \beta$ w/ $L_{ITE}$	29.0	52.5	15.4	13.6
	Ngram w/ $L_{ITE}$	22.2	49.9	14.1	12.9
	MLN-GT w/ $L_{ITE}$	-	33.7	12.3	11.8
	Attention w/ $L_{ITE}$	23.9	49.0	17.8	15.5
	OCRN w/ $L_{ITE}$	31.5	53.6	20.3	16.9

Table 2: OCL results. w/  $L_{ITE}$  means that training with ITE loss. The baselines in the upper block cannot operate ITE due to the model structure. Different  $\alpha$ - $\beta$  relations are exploited for causal graph comparison.

the significant difference between  $A$ ,  $B$  and  $\alpha$ ,  $\beta$ . Moreover, we find that all methods perform better on  $\beta$  than  $\alpha$ , and the improvement of OCRN on  $\alpha$  is larger too. This may be because  $\alpha$  are more diverse than  $\beta$ , e.g., we can eat lots of foods, but foods usually have various attributes (fruit vs. pizza). And OCL also has fewer attribute classes than affordance classes (114 vs. 170). Another reason is that the positive samples in  $\beta$  labels (23.2%) are much more than the positives in  $\alpha$  labels (9.4%). The different pos-neg ratio affects learning a lot and results in the above gap.

In ITE evaluation, without the guidance of  $L_{ITE}$ , all methods achieve unsatisfied performances. However, OCRN still has an advantage. Only MLN-GT adopting the first-order logic and GT  $\alpha$  labels is comparable with OCRN. If trained with  $L_{ITE}$  and direct causality labels, all methods perform much better to learn the causalities. Particularly, the typical deep learning model Attention performs best in baselines, but MLN-GT no longer holds the advantage. Relatively, OCRN shows more improvements and outperforms Attention with 2.5 and 1.4 mAP on two ITE tracks.

We provide more visualizations and discussions in the supplementary. In particular, we also apply OCRN to **Human-Object Interaction Detection** [53], where OCRN boosts the performances of multiple HOI models and verifies the generalization and application potential of OCL.

**Ablation Study.** We verify the components of OCRN w/  $L_{ITE}$  on the validation set in Tab. 3.

**Deconfounding.** OCRN w/o deconfounding is implemented following Eq. 3 and 5, where  $P(O|I)$  and

Method	$\alpha$	$\beta$	$\mathcal{S}_{ITE}$	$\mathcal{S}_{\alpha-\beta-ITE}$
OCRN	<b>32.4</b>	<b>52.2</b>	<b>20.5</b>	<b>17.0</b>
w/o deconfounding	32.1	51.8	18.2	16.1
w/o $L_{A_i}, L_{B_i}$	32.1	51.8	19.8	16.7
w/o $L_{\alpha}, L_{\beta}$	10.0	27.0	16.6	16.4
128 Dims	31.7	51.5	18.0	16.0
512 Dims	32.3	52.1	19.9	16.7
2048 Dims	32.2	51.5	19.1	16.3
Mean aggregation	32.2	51.3	18.9	16.7
Max-pooling aggregation	32.1	49.1	19.0	16.8
Random counterfactual	<b>32.4</b>	51.8	5.1	5.1

Table 3: Ablation study results (validation set).

$P(O|I, \alpha)$  are the category predictions of pre-trained detectors [68]. Both  $\alpha$  and  $\beta$  performances decline as the bias. For more bias analyses please refer to the supplementary.

**Losses.** The performances slightly drop after removing category-level  $L_{A_i}, L_{B_i}$ , but significantly drop without instance-level  $L_{\alpha}, L_{\beta}$ .

**Feature dimension.** For  $f_{A_i}, f_{B_i}, f_{\alpha}, f_{\beta}$ , smaller and larger feature sizes all have degrading effects.

**ITE-related implementations.** We probe some different methods: (a) Mean aggregation:  $f'_{\alpha} = \sum_i f_{\alpha_p}$ ; (b) Max-pooling aggregation:  $f'_{\alpha}$  is the max value of  $f_{\alpha_p}$  as each component; (c) Random counterfactual feature: assigned random vector as the counterfactual attribute feature (instead of zero vector) during ITE. These methods perform worse than the chosen setting on ITE performance but are comparable on  $\alpha$  and  $\beta$  performance.

**ITE Loss.** As shown in Tab. 2, the ITE loss significantly improves the accuracy of causal relations. It can also enhance  $\alpha$  and  $\beta$  learning. For DM- $\alpha \rightarrow \beta$  ITE loss leads to 1.0% improvement on  $\beta$  (79.9%→80.9%) on barely the samples with causal annotations.

**Discussion.** Overall, OCL poses extreme challenges to current AI systems. It expects representative learning to accurately recognize attributes and affordances from raw data meanwhile causal inference to capture the causalities within diverse instances and contexts, i.e., both the *intuitive System 1* and *logical System 2* [69]. From the experiments, we find that models struggle to achieve satisfying results on all tracks **simultaneously**. Notably, it is difficult to achieve a satisfying ITE score via data fitting. There is much room for improvement. For future studies, a harmonious performance on  $\alpha, \beta$ , and causality learning are encouraged to better capture object knowledge. Potential directions may include causal representation learning [70], neural-symbolic reasoning [71], and Foundation Models [72]. etc.

## 6. Conclusion

In this work, we introduce object concept learning (OCL) expecting machines to infer affordances and explain what attributes enable an object to possess them. Accord-



ingly, we build an extensive dataset and present OCRN based on casual intervention and instantiation. OCRN achieves decent performance and follows the causalities well. However, OCL remains challenging and would inspire a line of studies on reasoning-based object understanding.

## References

- [1] Jia Deng, Wei Dong, Richard Socher, Li-Jia Li, Kai Li, and Li Fei-Fei. Imagenet: A large-scale hierarchical image database. In *CVPR*, 2009. 1, 17
- [2] Tsung Yi Lin, Michael Maire, Serge Belongie, James Hays, Pietro Perona, Deva Ramanan, Piotr Dollár, and C. Lawrence Zitnick. Microsoft coco: Common objects in context. In *ECCV*, 2014. 1, 2, 7, 17, 22
- [3] Alex Krizhevsky, Ilya Sutskever, and Geoffrey E Hinton. Imagenet classification with deep convolutional neural networks. In *NIPS*, 2012. 1
- [4] Shaoqing Ren, Kaiming He, Ross Girshick, and Jian Sun. Faster r-cnn: Towards real-time object detection with region proposal networks. In *NIPS*, 2015. 1, 4
- [5] Phillip Isola, Joseph J Lim, and Edward H Adelson. Discovering states and transformations in image collections. In *CVPR*, 2015. 1, 2, 12
- [6] James J Gibson. *The ecological approach to visual perception: classic edition*. Psychology Press, 2014. 1, 2
- [7] Alex Martin. The representation of object concepts in the brain. *Annu. Rev. Psychol.*, 58:25–45, 2007. 1
- [8] Stevan Harnad. The symbol grounding problem. *Physica D: Nonlinear Phenomena*, 42(1-3):335–346, 1990. 1
- [9] B Ross. Category learning: Learning to access and use relevant knowledge. *Memory and mind: A Festschrift for Gordon H. Bower*, pages 229–246, 2008. 1
- [10] Christoph H Lampert, Hannes Nickisch, and Stefan Harmeling. Learning to detect unseen object classes by between-class attribute transfer. In *CVPR*, 2009. 1, 2
- [11] Jianxiong Xiao, James Hays, Krista A Ehinger, Aude Oliva, and Antonio Torralba. Sun database: Large-scale scene recognition from abbey to zoo. In *CVPR*, 2010. 1, 2, 3, 12, 17
- [12] Ali Farhadi, Ian Endres, Derek Hoiem, and David Forsyth. Describing objects by their attributes. In *CVPR*, 2009. 1, 2, 3, 12, 17
- [13] Thanh-Toan Do, Anh Nguyen, and Ian Reid. Affordancenet: An end-to-end deep learning approach for object affordance detection. In *ICRA*, 2018. 1, 2
- [14] Tucker Hermans, James M Rehg, and Aaron Bobick. Affordance prediction via learned object attributes. In *ICRA Workshop*, 2011. 1, 2, 3, 5
- [15] Ching-Yao Chuang, Jiaman Li, Antonio Torralba, and Sanja Fidler. Learning to act properly: Predicting and explaining affordances from images. In *CVPR*, 2018. 1, 2
- [16] Yuke Zhu, Alireza Fathi, and Li Fei-Fei. Reasoning about object affordances in a knowledge base representation. In *ECCV*, 2014. 1, 2, 3, 5, 12, 20, 28
- [17] Anh Nguyen, Dimitrios Kanoulas, Darwin G Caldwell, and Nikos G Tsagarakis. Object-based affordances detection with convolutional neural networks and dense conditional random fields. In *IROS*, 2017. 1, 2, 5, 12
- [18] David F Fouhey, Xiaolong Wang, and Abhinav Gupta. In defense of the direct perception of affordances. *arXiv preprint arXiv:1505.01085*, 2015. 1, 2, 5
- [19] Yu-Wei Chao, Zhan Wang, Rada Mihalcea, and Jia Deng. Mining semantic affordances of visual object categories. In *CVPR*, 2015. 2, 3, 12
- [20] Judea Pearl, Madelyn Glymour, and Nicholas P Jewell. *Causal inference in statistics: A primer*. John Wiley & Sons, 2016. 2, 3, 5, 14, 26, 28
- [21] Krishna Kumar Singh, Santosh Divvala, Ali Farhadi, and Yong Jae Lee. Dock: Detecting objects by transferring common-sense knowledge. In *ECCV*, 2018. 2
- [22] H. Liu, R. Wang, S. Shan, and X. Chen. Learning multifunctional binary codes for both category and attribute oriented retrieval tasks. In *CVPR*, 2017. 2, 3, 12
- [23] Genevieve Patterson and James Hays. Coco attributes: Attributes for people, animals, and objects. In *ECCV*, 2016. 2, 3, 12
- [24] Ranjay Krishna, Yuke Zhu, Oliver Groth, Justin Johnson, Kenji Hata, Joshua Kravitz, Stephanie Chen, Yannis Kalantidis, Li-Jia Li, David A Shamma, Michael Bernstein, and Li Fei-Fei. Visual genome: Connecting language and vision using crowdsourced dense image annotations. *IJCV*, 2016. 2, 12
- [25] Drew A Hudson and Christopher D Manning. Gqa: A new dataset for real-world visual reasoning and compositional question answering. In *CVPR*, 2019. 2
- [26] Devi Parikh and Kristen Grauman. Relative attributes. In *ICCV*, 2011. 2
- [27] Sung Ju Hwang, Fei Sha, and Kristen Grauman. Sharing features between objects and their attributes. In *CVPR*, 2011. 2
- [28] Chao-Yeh Chen and Kristen Grauman. Inferring analogous attributes. In *CVPR*, 2014. 2
- [29] Dhruv Mahajan, Sundararajan Sellamanickam, and Vinod Nair. A joint learning framework for attribute models and object descriptions. In *ICCV*, 2011. 2
- [30] Ishan Misra, Abhinav Gupta, and Martial Hebert. From red wine to red tomato: Composition with context. In *CVPR*, 2017. 2
- [31] Tushar Nagarajan and Kristen Grauman. Attributes as operators: factorizing unseen attribute-object compositions. In *ECCV*, 2018. 2
- [32] Yong-Lu Li, Yue Xu, Xiaohan Mao, and Cewu Lu. Symmetry and group in attribute-object compositions. *CVPR*, 2020. 2
- [33] Yong-Lu Li, Yue Xu, Xinyu Xu, Xiaohan Mao, and Cewu Lu. Learning single/multi-attribute of object with symmetry and group. *TPAMI*, 2021. 2
- [34] Yibiao Zhao and Song-Chun Zhu. Scene parsing by integrating function, geometry and appearance models. In *CVPR*, 2013. 2
- [35] Xiaolong Wang, Rohit Girdhar, and Abhinav Gupta. Binge watching: Scaling affordance learning from sitcoms. In *CVPR*, 2017. 2

- [36] Anirban Roy and Sinisa Todorovic. A multi-scale cnn for affordance segmentation in rgb images. In *ECCV*, 2016. [2](#)
- [37] Abhinav Gupta and Larry S Davis. Objects in action: An approach for combining action understanding and object perception. In *CVPR*, 2007. [2](#)
- [38] Bangpeng Yao, Jiayuan Ma, and Li Fei-Fei. Discovering object functionality. In *ICCV*, 2013. [2](#)
- [39] Keizo Kato, Yin Li, and Abhinav Gupta. Compositional learning for human object interaction. In *ECCV*, 2018. [2](#)
- [40] Lerrel Pinto and Abhinav Gupta. Supersizing self-supervision: Learning to grasp from 50k tries and 700 robot hours. In *ICRA*, 2016. [2](#)
- [41] Spyridon Thermos, Georgios Th Papadopoulos, Petros Daras, and Gerasimos Potamianos. Deep affordance-grounded sensorimotor object recognition. In *CVPR*, 2017. [2](#)
- [42] Lerrel Pinto, Dhiraj Gandhi, Yuanfeng Han, Yong-Lae Park, and Abhinav Gupta. The curious robot: Learning visual representations via physical interactions. In *ECCV*, 2016. [2](#)
- [43] Peter Spirtes, Clark N Glymour, Richard Scheines, and David Heckerman. *Causation, prediction, and search*. MIT press, 2000. [2](#)
- [44] Isabelle Guyon, Constantin Aliferis, and André Elisseeff. Causal feature selection. *Computational methods of feature selection*, pages 63–82, 2007. [2](#)
- [45] Krzysztof Chalupka, Pietro Perona, and Frederick Eberhardt. Visual causal feature learning. *arXiv preprint arXiv:1412.2309*, 2014. [2](#)
- [46] Lyndsey C Pickup, Zheng Pan, Donglai Wei, YiChang Shih, Changshui Zhang, Andrew Zisserman, Bernhard Schölkopf, and William T Freeman. Seeing the arrow of time. In *CVPR*, 2014. [2](#)
- [47] Karel Lebeda, Simon Hadfield, and Richard Bowden. Exploring causal relationships in visual object tracking. In *ICCV*, 2015. [2](#)
- [48] Suraj Nair, Yuke Zhu, Silvio Savarese, and Li Fei-Fei. Causal induction from visual observations for goal directed tasks. *arXiv preprint arXiv:1910.01751*, 2019. [2](#)
- [49] Ishita Dasgupta, Jane Wang, Silvia Chiappa, Jovana Mitrovic, Pedro Ortega, David Raposo, Edward Hughes, Peter Battaglia, Matthew Botvinick, and Zeb Kurth-Nelson. Causal reasoning from meta-reinforcement learning. *arXiv preprint arXiv:1901.08162*, 2019. [2](#)
- [50] Tan Wang, Jianqiang Huang, Hanwang Zhang, and Qianru Sun. Visual commonsense r-cnn. In *CVPR*, 2020. [2](#), [5](#), [19](#), [27](#), [28](#)
- [51] Yuval Atzmon, Felix Kreuk, Uri Shalit, and Gal Chechik. A causal view of compositional zero-shot recognition. *arXiv preprint arXiv:2006.14610*, 2020. [2](#)
- [52] Chunhui Gu, Chen Sun, David A Ross, Carl Vondrick, Caroline Pantofaru, Yeqing Li, Sudheendra Vijayanarasimhan, George Toderici, Susanna Ricco, Rahul Sukthankar, Cordelia Schmid, and Jitendra Malik. Ava: A video dataset of spatio-temporally localized atomic visual actions. In *CVPR*, 2018. [2](#), [12](#)
- [53] Yu-Wei Chao, Yunfan Liu, Xieyang Liu, Huayi Zeng, and Jia Deng. Learning to detect human-object interactions. In *WACV*, 2018. [2](#), [8](#), [12](#), [23](#), [24](#), [26](#)
- [54] Saurabh Gupta and Jitendra Malik. Visual semantic role labeling. *arXiv preprint arXiv:1505.04474*, 2015. [2](#), [12](#), [24](#)
- [55] Christiane Fellbaum. Wordnet. *The encyclopedia of applied linguistics*, 2012. [2](#), [12](#)
- [56] Daniel N Osherson, Joshua Stern, Ormond Wilkie, Michael Stob, and Edward E Smith. Default probability. *Cognitive Science*, 15(2):251–269, 1991. [3](#), [12](#)
- [57] Robin Rombach, Andreas Blattmann, Dominik Lorenz, Patrick Esser, and Bjorn Ommer. High-resolution image synthesis with latent diffusion models. In *CVPR*, 2022. [4](#)
- [58] Donald B Rubin. Causal inference using potential outcomes: Design, modeling, decisions. *Journal of the American Statistical Association*, 100(469):322–331, 2005. [4](#), [6](#), [18](#)
- [59] Agrim Gupta, Piotr Dollar, and Ross Girshick. Lvis: A dataset for large vocabulary instance segmentation. In *CVPR*, 2019. [4](#)
- [60] Yue Xu, Yong-Lu Li, Jiefeng Li, and Cewu Lu. Constructing balance from imbalance for long-tailed image recognition. In *ECCV*, 2022. [4](#)
- [61] Kaiming He, Xiangyu Zhang, Shaoqing Ren, and Jian Sun. Deep residual learning for image recognition. In *CVPR*, 2016. [5](#), [7](#)
- [62] Ashish Vaswani, Noam Shazeer, Niki Parmar, Jakob Uszkoreit, Llion Jones, Aidan N Gomez, Łukasz Kaiser, and Illia Polosukhin. Attention is all you need. In *Advances in neural information processing systems*, pages 5998–6008, 2017. [5](#)
- [63] Kaihua Tang, Yulei Niu, Jianqiang Huang, Jiaxin Shi, and Hanwang Zhang. Unbiased scene graph generation from biased training. In *CVPR*, 2020. [6](#), [19](#), [21](#), [27](#), [28](#)
- [64] Jacob Devlin, Ming-Wei Chang, Kenton Lee, and Kristina Toutanova. Bert: Pre-training of deep bidirectional transformers for language understanding. *arXiv preprint arXiv:1810.04805*, 2018. [7](#), [19](#)
- [65] Tinghui Zhou, Hanhuai Shan, Arindam Banerjee, and Guillermo Sapiro. Kernelized probabilistic matrix factorization: Exploiting graphs and side information. In *SDM*, 2012. [7](#), [19](#)
- [66] Y. Lin, J.-B. Michel, E. L. Aiden, J. Orwant, W. Brockman, and S. Petrov. Syntactic annotations for the google books ngram corpus. In *ACL*, 2012. [7](#), [20](#)
- [67] Matthew Richardson and Pedro Domingos. Markov logic networks. *Machine learning*, 62(1-2):107–136, 2006. [7](#), [20](#)
- [68] Ze Liu, Yutong Lin, Yue Cao, Han Hu, Yixuan Wei, Zheng Zhang, Stephen Lin, and Baining Guo. Swin transformer: Hierarchical vision transformer using shifted windows. *arXiv preprint arXiv:2103.14030*, 2021. [8](#), [22](#), [25](#)
- [69] Yoshua Bengio. From system 1 deep learning to system 2 deep learning. In *Posner lecture at NeurIPS’2019*, 2019. [8](#)
- [70] Bernhard Schölkopf, Francesco Locatello, Stefan Bauer, Nan Rosemary Ke, Nal Kalchbrenner, Anirudh Goyal, and Yoshua Bengio. Toward causal representation learning. *Proceedings of the IEEE*, 109(5):612–634, 2021. [8](#)
- [71] Tarek R Besold, Artur d’Avila Garcez, Sebastian Bader, Howard Bowman, Pedro Domingos, Pascal Hitzler, Kai-Uwe Kühnberger, Luis C Lamb, Daniel Lowd, Priscila Machado Vieira Lima, et al. Neural-symbolic learning and reasoning: A survey and interpretation. *arXiv preprint arXiv:1711.03902*, 2017. [8](#)

- [72] Long Ouyang, Jeff Wu, Xu Jiang, Diogo Almeida, Carroll L Wainwright, Pamela Mishkin, Chong Zhang, Sandhini Agarwal, Katarina Slama, Alex Ray, et al. Training language models to follow instructions with human feedback. *arXiv preprint arXiv:2203.02155*, 2022. 8
- [73] Zhenliang He, Wangmeng Zuo, Meina Kan, Shiguang Shan, and Xilin Chen. Attgan: Facial attribute editing by only changing what you want. *TIP*, 2019. 15
- [74] Laurens van der Maaten and Geoffrey Hinton. Visualizing data using t-sne. *JMLR*, 2008. 16
- [75] Kaihua Tang, Jianqiang Huang, and Hanwang Zhang. Long-tailed classification by keeping the good and removing the bad momentum causal effect. *arXiv preprint arXiv:2009.12991*, 2020. 19, 27, 28
- [76] Jimmy Lei Ba, Jamie Ryan Kiros, and Geoffrey E. Hinton. Layer normalization, 2016. 19
- [77] Tomas Mikolov, Kai Chen, Greg Corrado, and Jeffrey Dean. Efficient estimation of word representations in vector space. *arXiv preprint arXiv:1301.3781*, 2013. 20
- [78] Yong-Lu Li, Hongwei Fan, Zuoyu Qiu, Yiming Dou, Liang Xu, Hao-Shu Fang, Peiyang Guo, Haisheng Su, Dongliang Wang, Wei Wu, and Cewu Lu. Discovering a variety of objects in spatio-temporal human-object interactions. *arXiv preprint arXiv:2211.07501*, 2022. 23
- [79] Yong-Lu Li, Liang Xu, Xinpeng Liu, Xijie Huang, Yue Xu, Shiyi Wang, Hao-Shu Fang, Ze Ma, Mingyang Chen, and Cewu Lu. Pastanet: Toward human activity knowledge engine. In *CVPR*, 2020. 23
- [80] Yong-Lu Li, Xinpeng Liu, Xiaoqian Wu, Xijie Huang, Liang Xu, and Cewu Lu. Transferable interactiveness knowledge for human-object interaction detection. In *TPAMI*, 2022. 23
- [81] Xinpeng Liu, Yong-Lu Li, and Cewu Lu. Highlighting object category immunity for the generalization of human-object interaction detection. In *AAAI 2022*, 2022. 23
- [82] Hao-Shu Fang, Yichen Xie, Dian Shao, Yong-Lu Li, and Cewu Lu. Decaug: Augmenting hoi detection via decomposition. In *AAAI*, 2021. 23
- [83] Xinpeng Liu, Yong-Lu Li, Xiaoqian Wu, Yu-Wing Tai, Cewu Lu, and Chi-Keung Tang. Interactiveness field in human-object interactions. In *CVPR*, 2022. 23
- [84] Xiaoqian Wu, Yong-Lu Li, Xinpeng Liu, Junyi Zhang, Yuzhe Wu, and Cewu Lu. Mining cross-person cues for body-part interactiveness learning in hoi detection. In *ECCV*, 2022. 23
- [85] Yong-Lu Li, Xinpeng Liu, Han Lu, Shiyi Wang, Junqi Liu, Jiefeng Li, and Cewu Lu. Detailed 2d-3d joint representation for human-object interaction. In *CVPR*, 2020. 23
- [86] Xinyu Xu, Yong-Lu Li, and Cewu Lu. Learning to anticipate future with dynamic context removal. In *CVPR*, 2022. 23
- [87] Yong-Lu Li, Liang Xu, Xinpeng Liu, Xijie Huang, Yue Xu, Mingyang Chen, Ze Ma, Shiyi Wang, Hao-Shu Fang, and Cewu Lu. Hake: Human activity knowledge engine. *arXiv preprint arXiv:1904.06539*, 2019. 24
- [88] Yong-Lu Li, Xinpeng Liu, Xiaoqian Wu, Yizhuo Li, Zuoyu Qiu, Liang Xu, Yue Xu, Hao-Shu Fang, and Cewu Lu. Hake: A knowledge engine foundation for human activity understanding. *TPAMI*, 2023. 24
- [89] Yong-Lu Li, Siyuan Zhou, Xijie Huang, Liang Xu, Ze Ma, Hao-Shu Fang, Yanfeng Wang, and Cewu Lu. Transferable interactiveness knowledge for human-object interaction detection. In *CVPR*, 2019. 24, 25, 26
- [90] Chen Gao, Yuliang Zou, and Jia-Bin Huang. ican: Instance-centric attention network for human-object interaction detection. In *BMVC*, 2018. 24, 25, 26
- [91] Yong-Lu Li, Xinpeng Liu, Xiaoqian Wu, Yizhuo Li, and Cewu Lu. Hoi analysis: Integrating and decomposing human-object interaction. In *NeurIPS*, 2020. 24, 26
- [92] Zeyu Wang, Klint Qinami, Ioannis Christos Karakozis, Kyle Genova, Prem Nair, Kenji Hata, and Olga Russakovsky. Towards fairness in visual recognition: Effective strategies for bias mitigation. In *CVPR*, 2020. 27
- [93] Jieyu Zhao, Tianlu Wang, Mark Yatskar, Vicente Ordonez, and Kai-Wei Chang. Men also like shopping: Reducing gender bias amplification using corpus-level constraints. *arXiv preprint arXiv:1707.09457*, 2017. 27
- [94] Patricia W Cheng and Laura R Novick. Causes versus enabling conditions. *Cognition*, 40(1-2):83–120, 1991. 28

We report more details and analyses here:

Sec. **A**: Category/Attribute/Affordance Selection

Sec. **B**: Annotation Details

Sec. **C**: Causal Graph

Sec. **D**: OCL Characteristics

Sec. **E**: ITE Metric Details

Sec. **F**: Baseline Details

Sec. **G**: Detailed Result Analysis

Sec. **H**: Application on HOI Detection

Sec. **I**: Comparison on Debiasing

Sec. **J**: Discussion about States

Sec. **K**: Discussion about Causality and Causal Graph

## A. Category/Attribute/Affordance Selection

We choose affordances, categories, and attributes, considering their causal relations. Their word clouds are shown in Fig. 7.

(1) **Affordance**: To build a general and applicable knowledge base, we collect 1,006 affordance candidates from several widely-used action/affordance datasets: 957 from [19], 160 from [52], 146 from [53], 97 from [54], 41 from [16], 21 from [17] (with *overlaps*). We find that not all affordances are in common use and some of them are difficult for visual recognition, *e.g.*, *accept* (consider right and proper). So each candidate is scored by 5 human experts from 0.0 to 5.0 according to generality and commonness. We keep **170** top-scored affordances in our base (134 from [19], 78 from [52], 127 from [53], 53 from [54], 13 from [16], 11 from [17], with *overlaps*).

(2) **Category**: Considering the taxonomy (WordNet [55]), we collect a pool with over 1,742 object categories from previous datasets: 32 from [12], 28 from [23], 717 from [11], 1,000 from [22] (with *overlaps*). Then we merge the similar categories according to WordNet [55] and filter out the categories which are not common daily objects (man, planet), unrelated to the above 170 affordances (skyscraper) or too uncommon (malleeowl). Finally, our database has **381** common object categories. These object categories are divided into **12** super categories, shown in Fig. 8.

(3) **Attribute**: We extract the attributes from several large-scale attribute datasets: 64 from [12], 203 from [23], 66 from [11], 25 from [22], top 500 from [24]), and manually filter the 500 most frequent attributes. Five experts give 0 to 5 scores based on their relevance to human actions and the selected 170 affordances to better explore the causal relations between attributes and affordances. Some attributes (cloudy, competitive) that are not useful for affordance reasoning are discarded. Finally, **114** attributes are kept, covering colors, deformations, supercategories, surface, geometrical, and physical properties.

## B. Annotation Details

### B.1. Attribute Annotation

(1) **Category-level attribute** ( $A$ ). Following [56], to avoid bias, annotators are given *category-attribute pairs* (category *names*, not images). They propose a 0-3 score according to the category concept in their minds (0: No, 1: Normally No, 2: Normally Yes, 3: Yes). Each pair is annotated by three annotators and takes the plurality as the  $A$  label. If the range of 3 proposals exceeds 1, another three annotators will re-annotate this pair until achieving consensus. We binarize the annotations (0: No, 1: Yes) with a threshold of 2 and get a category-level attribute matrix  $M_A$  ([381, 114]).

(2) **Instance-level attribute** ( $\alpha$ ). Two annotators label each pair with 0 (No) and 1 (Yes). If they give different labels, this pair will be handed over to another two annotators until meeting consensus.

### B.2. Affordance Annotation

(1) **Category-level affordance**  $B$ . Following [19], the annotators are given category-affordance pairs. The pairs are annotated in four bins (0-3) and normalized (same as  $A$ ) to describe the possibility of an affordance in a category. Each pair is annotated by three annotators and makes consensus the same as  $A$ . The 0-3 scores are binarized (1: Yes, 0: No) with a threshold of 2. The final category-level affordance matrix  $M_B$  is [381, 170].

(2) **Instance-level affordance**  $\beta$  is annotated for **every instance** with the help of *object states* [5]. As  $B$  is determined by common states, objects in specific states may have different affordances from  $B$ , *e.g.*, we cannot board a flying plane. As the instances in the same state should have similar  $\beta$  (all rotten apples cannot be eaten), six experts first conclude the states. The experts scan all instances of each category and use their knowledge of affordance to define all the existing states. Then all 186 K instances are dispatched to the concluded states via crowdsourcing. If some instances do not belong to any predefined states, they will be returned to the experts to add more states. In total, **1,376** states are defined, and each category has 3.6 states on average. Next,  $\beta$  is annotated for each state. Given a *state-affordance pair* and example images, two annotators mark it with 0 (No) and 1 (Yes). The results are combined in the same way as  $\alpha$ . Thus, each instance would have a state and the corresponding  $\beta$ . An annotator would recheck each instance together with its state and  $\beta$  labels to ensure the quality. If its state is inaccurate or the state  $\beta$  labels are unsuitable, this annotator would correct them.





Figure 7: Word clouds of object categories, attributes, and affordance (by positive frequencies in OCL).

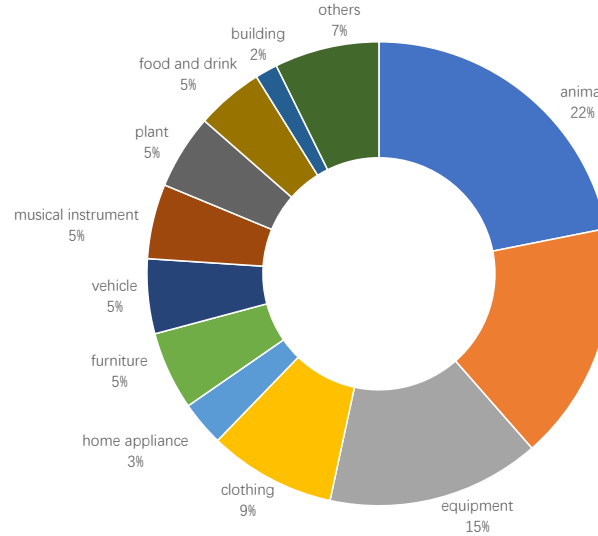


Figure 8: Super-categories of objects in OCL.

### B.3. Causal Relation Annotation

(1) **Filtering.** Starting from the  $[114,170]$  matrix of  $\alpha$ - $\beta$  classes, we ask three experts to vote on the causal relation of each class. They scan all instances to answer whether the relationship exists in any case. That is, we just annotate the *least* pairs with the *largest* possibility to be casually related. Some causal pairs may be excluded. The pairs we selected are checked carefully to ensure the causalities and we only evaluate models on them. Thus, the missed causal pairs or non-causal pairs would not affect the results. Finally, we obtain about 10%  $\alpha$ - $\beta$  classes as candidates.

(2) **Instance-level causality:** we also adopt object states as a reference. For each *state*- $\alpha$ - $\beta$  triplet, two annotators are asked whether the specific attribute is the *direct* and *unambiguous* cause of this affordance in this state and gives their binary answer. We use the same method in annotating  $\beta$  to combine results and assign *state-level* labels to instances. Next, for all instances of a state, an expert decides whether the state-level relations are reasonable for each *instance* in specific contexts and correct the inaccurate ones. Finally, we obtain about 2 M *instance*- $\alpha$ - $\beta$  triplets of causal relations.

### B.4. A Running Example of Dataset Construction.

A running example is shown in Fig. 9 to show the process of annotations clearly.

## C. Causal Graph

In this section, we first briefly introduce the causal graph model and causal intervention. Then we introduce the details of the causal graph our knowledge base can support. Then, we detail the implementation of the causal graphs used by different methods.

### C.1. Basics of Causal Inference and Causal Graph

A causal graph is a DAG that describes the causal relations between multiple factors. Each directed edge points from the “cause” to its “effect”, e.g. in Fig. 11, node  $X$  is the cause of node  $Y$ . Under the scenario that causal variables and causal graphs are known, **causal inference** studies how to infer the strength of causal edges given observations, or infer the outcomes given some of the causal variable values.

However, the causal relation in the real world is sophisticated. The causal relation that we observed may have been polluted by spurious variables. For example, let  $X$

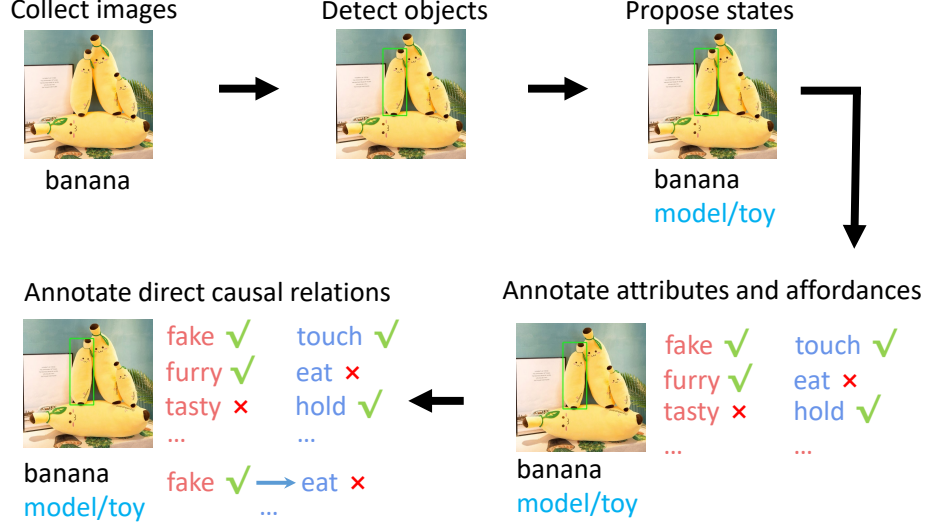


Figure 9: A running example of dataset construction.

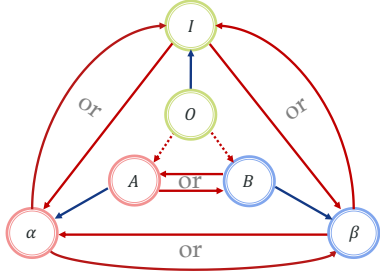


Figure 10: A more complex causal graph of our knowledge base.  $A, B, O$  are the object category and category-level attribute and affordance.  $I$  is the object appearance,  $\alpha, \beta$  are the instance-level attribute and affordance. Note that “or” indicates that the arcs between  $A, B, \alpha, \beta, I, \alpha$  and  $I, \beta$  indicate that either  $A \leftarrow B$  or  $A \rightarrow B$  (the others are similar) is considering in the setting.

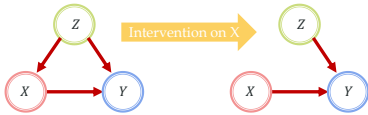


Figure 11: An example of the causal graph and causal intervention. We study the causal relation  $X \rightarrow Y$  while confounder  $Z$  exists and brings bias. After the intervention on variable  $X$ , the poisonous relation  $Z \rightarrow X$  is eliminated.

in Fig. 11 be ice cream sales and  $Y$  be drownings, one may observe that more ice cream sales lead to more drownings and infer that they are causally related. Actually, the observed relation is due to another factor  $Z$ : weather temperature. These variables are called **confounders**, which is the common cause of two causal variables that we are studying, e.g. in the left graph in Fig. 11,  $Z$  is a confounder when we focus on the causal edge  $X \rightarrow Y$ .

In causal inference, confounders should be eliminated to avoid biases on causal learning, by applying **intervention** on the cause variables (e.g.  $X$  in our example) to “control” its distribution to block the effect of confounder. Traditional scientific research on causality adopts Randomized Controlled Trial (RCT) to completely remove the confounder, but it is not applicable when we only have observational data. Pearl. [20] et al. propose *do-calculus* to systematically analyze the causal graph and alleviate the confounder bias in a probabilistic view. In the simple case in Fig. 11, the confounder  $Z$  can be eliminated with **Back-door Adjustment**:

$$P(Y|do(X)) = \sum_z P(Y|X, Z = z)P(Z = z), \quad (12)$$

where  $z$  is the specific value of the random variable  $Z$ . The causal graph of our OCRN also meets the back-door criterion so we apply the back-door adjustment to alleviate bias from the confounder  $O$ .

## C.2. Causal Graph of Our Knowledge Base

A more complicated causal graph considering more arcs between nodes is shown in Fig. 10. The causal relations between nodes or arcs in Fig. 10 are determined as follows:

Firstly, we introduce two kinds of special arcs.

$O \rightarrow A, O \rightarrow B$  (dotted arcs): in OCL,  $A$  and  $B$  are defined as the category-level annotations. Given  $O, A$ , and  $B$  are strictly determined. In Fig. 10, we use two dotted arrows from  $O$  to  $A, B$  respectively to indicate this deterministic relation to distinguish them from the other causal relations.

$O \rightarrow I, A \rightarrow \alpha, B \rightarrow \beta$  (blue arcs): we see the category-level  $O, A$ , and  $B$  are direct causes of instance-level  $I, \alpha$ , and  $\beta$  during the concept *instantiation* according

to OCL definition. Because the visual representation  $I$  and properties  $\alpha, \beta$  of an instance are derived from the concept-level categorical ones. The reversed arcs  $O \leftarrow I, A \leftarrow \alpha, B \leftarrow \beta$  mean that  $O, A, B$  are the *aggregations* of instances and would be marginally affected by one specific instance, thus we do not include these arcs here for clarity.

Next, we illustrate the regular causal arcs as follows.

$I \rightarrow \alpha, I \rightarrow \beta$ : the recognition process of  $\alpha$  and  $\beta$ . As  $I$  indicates the *physical noumenon*, it is the source of semantic and functional properties and decides/causes  $\alpha, \beta$ .

$\alpha \rightarrow I, \beta \rightarrow I$ : the generation of visual pattern from attribute or affordance descriptions and can be utilized in image generation/manipulation tasks [73].

$A \leftarrow B$  or  $A \rightarrow B, \alpha \leftarrow \beta$  or  $\alpha \rightarrow \beta$ : the causal direction between attribute and affordance can be reversed sometimes. The arc from  $\alpha$  to  $\beta$  is evident, e.g., a broken cup is not useable. Sometimes, the reverse arc causal effect from  $\beta$  to  $\alpha$  also exists, e.g., an eatable banana would not be unripe.

### C.3. Causal Graph Implementation

In this work, we mainly study the recognition and reasoning of attribute and affordance for robotics and embodied AI, hence we remove the two arcs corresponding to image generation  $\alpha \rightarrow I, \beta \rightarrow I$ . Due to the deterministic relation between  $O, A$ , and  $B$ , we can simplify the three nodes to a single node  $O'$  (Fig. 12).

Different *methods* can exploit different causal paths. We propose diverse baselines to implement different causal subgraphs, including the subgraphs with  $\alpha \rightarrow \beta$ , and  $\alpha \leftarrow \beta$ . The causal graphs of some baselines are shown in Fig. 13.

The ablation experiment with arc  $\alpha \rightarrow \beta$  and  $\alpha \leftarrow \beta$  shows that the causal effect of  $\alpha \rightarrow \beta$  is stronger than the alternative in our datasets. Besides, from the aspect of embodied AI and robotics, affordance is more important in practical applications like object manipulation, so we focus more on affordance recognition and regard  $\beta$  inference as our main goal. Therefore, in OCRN and some other baselines, we keep the arc  $\alpha \rightarrow \beta$ . And in causal reasoning, we focus on the evaluation of  $\alpha \rightarrow \beta$  too. The causal graph of OCRN is shown in Fig. 14.

## D. OCL Characteristics

### D.1. Object Box Size

We visualize the distribution of normalized object box size in Fig. 15, where the box width and height are normalized by the width and height of the whole image. It shows that most objects in our knowledge base are *small objects*, providing abundant regional information.

### D.2. Annotator Information

Annotators' age, major, and education degree are presented in Fig. 16, 17, and 18.

### D.3. Matrix Samples

The category-level attribute and affordance ( $A, B$ ) matrices are detailed in Fig. 19, 20 as heatmaps, and the cells with dark color indicate positive samples. For example, ice cream is cold while clock is not natural, cake can be eaten while eraser can not be cooked. These are in line with our common sense.

### D.4. State Distribution

Before annotating the affordances, we first define the object states for all object categories and annotate the state affordances. In total, we define 1,376 states for 381 object categories. And Fig. 21 shows the state distribution per object category.

### D.5. Attribute-Affordance Relation

We analyze the instance-level attribute-affordance relations in our knowledge base under three criteria. (1) **Attribute Conditioned Affordance Probability**. It is computed as  $P(\beta|\alpha)$  to estimate affordance probability given an attribute. The range is [0,1]. (2) **Attribute-Affordance Correlation**. For all instances in our dataset, we evaluate the label correlation of each attribute-affordance pair, whose scale is in [-1,1]. (3) **Attribute-Affordance Causality**. Starting with the annotated cause-effect ( $\alpha - \beta$ ) labels, we count for how many times each attribute-affordance pair appear in our dataset and normalize the value by the maximum occurrences, leading to a value in the range [0,1]. It should be mentioned that we only annotate whether an attribute-affordance pair **has** explicit and key causality, but the detailed effect (**positive** or **negative**) should be referred to instance labels.

We visualize the samples of attribute-affordance relation matrices in Fig. 22, 23, 24 and observe some interesting properties of them. They reveal some common relations, such as what is between *tasty* and *eat*. However, some of the criteria suffer from data bias. For the condition matrix in Fig. 22, it only cares about cases with *positive* attribute labels, which is not good in highlighting the negative relations, e.g., the relation between *natural* and *produce*. For the former two matrices in Fig. 22, 23, they all point out the relation between *tasty* and *pick*, since most *tasty* objects are *pickable food*. This finding is simply misled by the data bias but violates the causal graph (inference from attribute to object category, then affordance). Last, the matrix obtained from our causal annotation in Fig. 24 is more sparse and clear of causality.

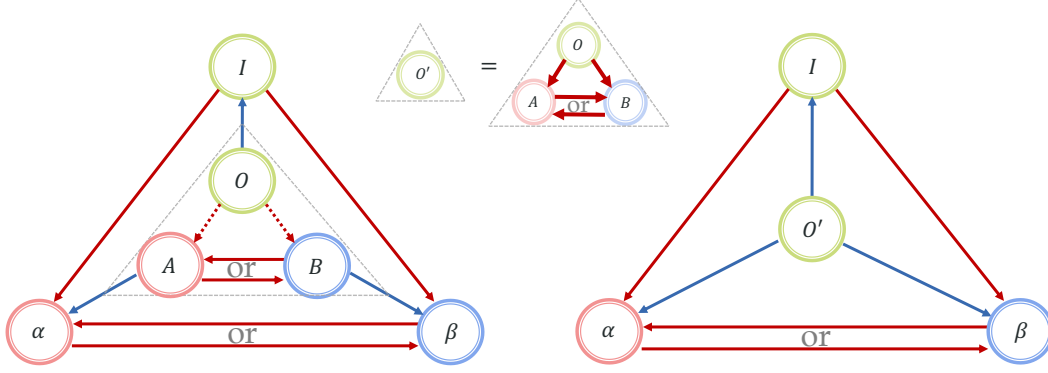


Figure 12: Simplified causal graph for OCL task. Note that “or” indicates that the arcs between  $A, B$  and  $\alpha, \beta$  are either  $A \leftarrow B$  or  $A \rightarrow B$  ( $\alpha \leftarrow \beta$  or  $\alpha \rightarrow \beta$ ), instead of concurrence.

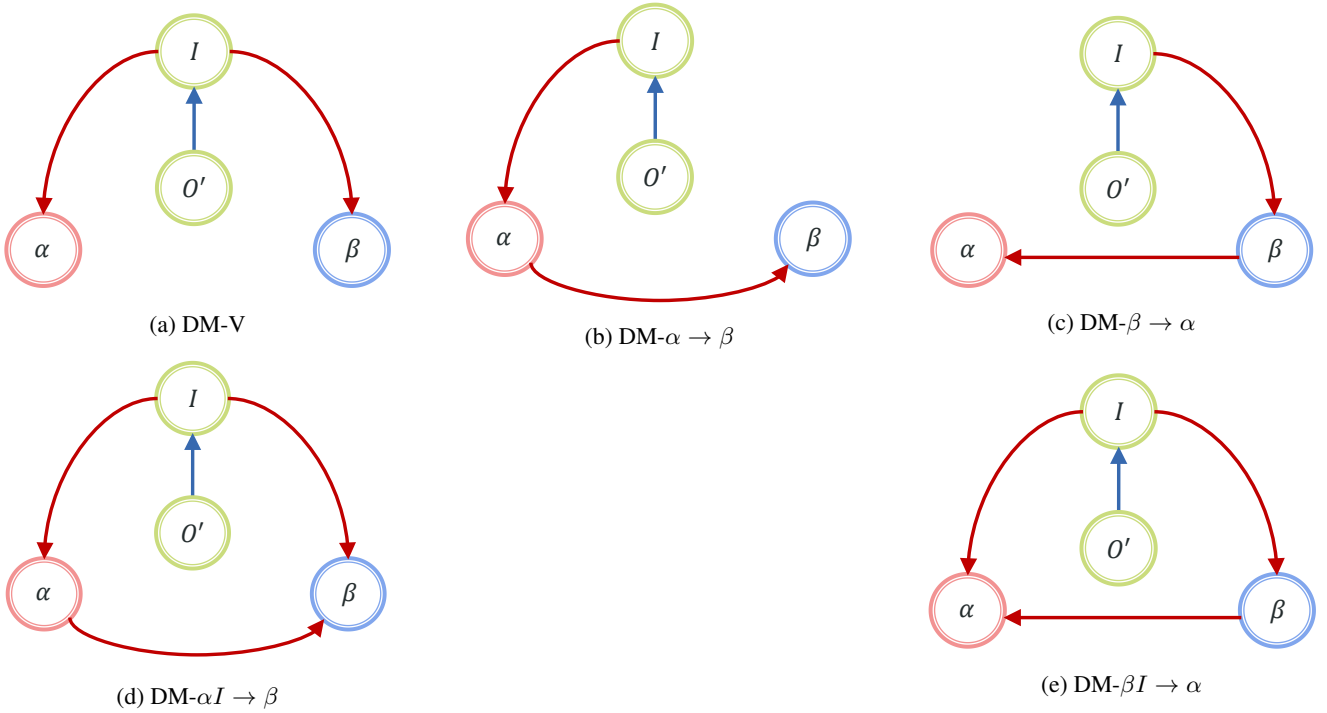


Figure 13: Causal graphs of the baselines.

## D.6. Unified Object Representation

To compare the difference between attribute-only and attribute-affordance representations, we cluster the object instances of two similar animals (zebra and horse) with their attribute labels and attribute-affordance labels, respectively. The results are shown in Fig. 25 via t-SNE [74]. With both attribute and affordance labels, zebra and horse can be better separated than attribute only. And attribute and affordance together can differentiate specific **states** well, such as *riding, pulling car*, etc.

## D.7. Difference between Category- and Instance-Level Labels

We analyze the differences between category-level  $A, B$  labels and instance-level  $\alpha, \beta$  labels. For each object category, we compute the *average ratio* of changed attribute/affordance classes during each instantiation from  $A$  to  $\alpha$  or from  $B$  to  $\beta$ . The top 50 categories with the most significant differences between  $A$  and  $\alpha$  as well as  $B$  and  $\beta$  are reported respectively in Fig. 26. We find that affordance labels change more dramatically than attribute labels during instantiations. This is because **each** attribute change



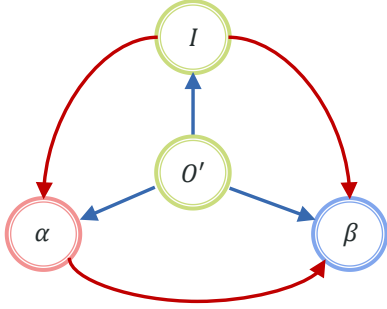


Figure 14: Causal graph of OCRN.

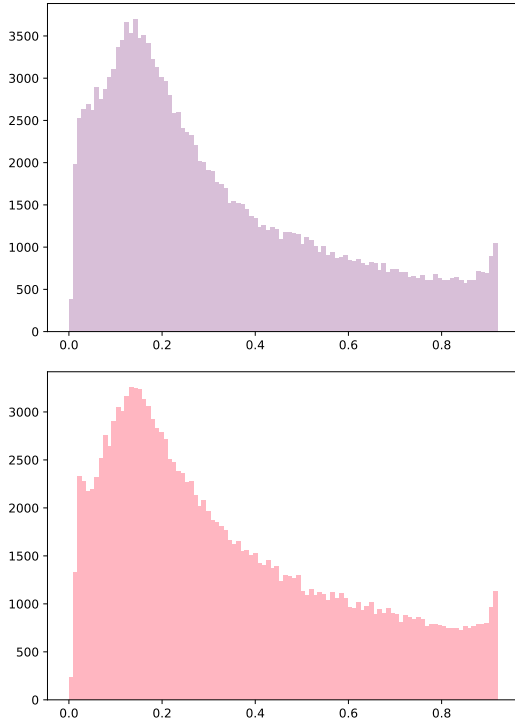


Figure 15: Distribution of normalized object box width (left) and height (right).

may affect **several** affordances, *e.g.*, when a common book becomes burning, we can neither open nor read it.

### D.8. Attribute-Affordance Causal Relations

We annotate all object instances’ causal relations of filtered  $[\alpha_p, \beta_q]$  pairs. In total, 1,085  $[\alpha_p, \beta_q]$  pairs are chosen for the causality annotation, and over 2 M *instance- $\alpha$ - $\beta$*  triplets are annotated. In the ITE evaluation (main text Sec. 5), we report the mean AP of top-300  $[\alpha_p, \beta_q]$  pairs to avoid the biased influence of very rare  $[\alpha_p, \beta_q]$  pairs that include less than 35 object instances.

### D.9. Data Partitioning

For the OCL task, our knowledge base is split into the train, val, and test sets. The statistical details of the split are listed in Tab. 4. The image number ratio of the three sets is nearly 4:1:0.6, and the instance ratio is around 5:1:1.

Set	Image	Object Instance	Object category
Train	56,916	135,148	381
Val	14,446	25,176	221
Test	9,101	25,617	221
Val+Test	23,547	50,793	221
All	80,463	185,941	381

Table 4: Detailed data split of our knowledge base.

### D.10. Images and Instances

Some additional data samples of our knowledge base are shown in Fig. 27, 28a, 28b, 29, and 30, including samples of diverse object categories with various bounding box distributions, different attributes and affordances, and human-labeled object states and obvious causal relations. We also show the counts of object categories, attributes, and affordances in instance/image in Fig. 31, 32, and 33.

### D.11. More Statistics of Annotation

We divide  $A, B, \alpha, \beta$ , causality annotation into multiple finer-grained small sets in our pipeline. Generally, we have 13, 19, 124, 140, and 85 annotator sets (381 total) for  $A, B, \alpha, \beta$ , and causality annotation respectively. We assign each small set to 2 annotators. However, considering the controversial situations introduced, part of the annotation are confused cases based on their results. In the whole process, 9.6% of  $A$ , 7.7% of  $B$ , 5.2% of  $\alpha$ , 7.9% of  $\beta$ , and 13.7% of causality are confusing and re-assigned to additional annotators. These indeterminable ones will be sent to two extra annotators until agreement. The quality of the dataset is guaranteed by a low confusion ratio and multiple refining stages.

### D.12. Potential Bias

We have considered the bias issue in the construction of our dataset. (1) In our dataset, the existing datasets (ImageNet [1], COCO [2], aPY [12], SUN [11]) are open-sourced datasets and the images collected from the Internet are publicly accessible too. The dataset is constructed for only non-commercial purposes. We will only provide the URLs of these images to avoid copyright infringement. (2) During image collection, we choose images with general objects and are particularly careful with the image selection to avoid unsuitable content, private images, or implicit biases. (3) During annotation, the annotators cover different

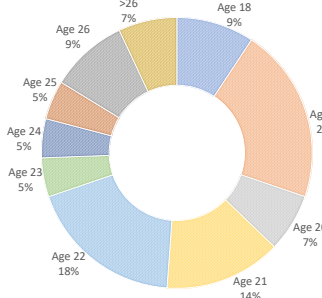


Figure 16: Age information of annotators.

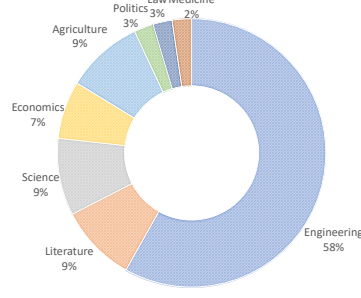


Figure 17: Major information of annotators.

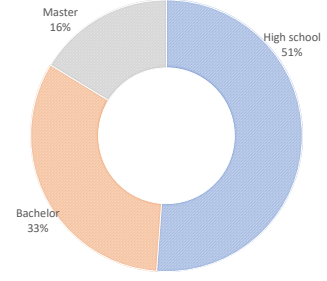


Figure 18: Degree information of annotators.

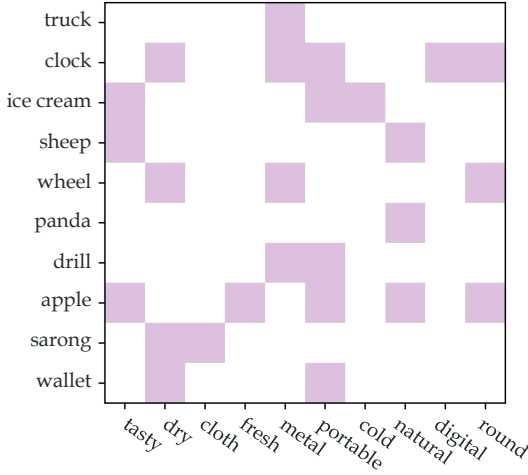


Figure 19: Category-level attribute (A) matrix.

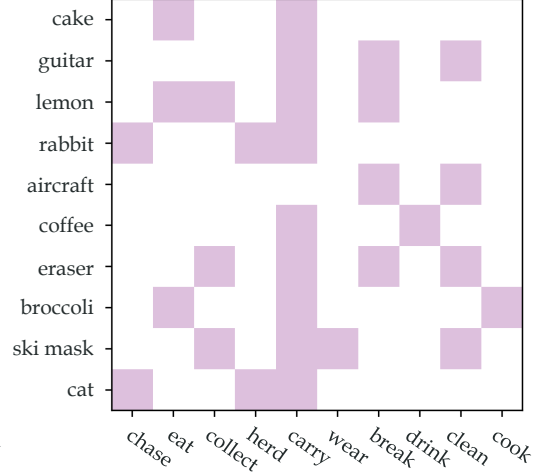


Figure 20: Category-level affordance (B) matrix.

genders, ages, and fields of expertise to avoid potential annotation biases. And they are all informed on how we will use the annotations in our research.

## E. ITE Metric Details

ITE (**I**ndividual **T**reatment **E**ffect (**ITE**) [58]) is to measure whether a model infers affordance with proper attention to the causality-related attribute. That said, when removing the attribute, the model is expected to have *large prediction difference further away from the ground truth*.

We detail some settings in our ITE metric. For the ITE score:

$$\mathcal{S}_{\text{ITE}} = \begin{cases} \max(\Delta\hat{\beta}_q, 0), & \beta_q = 1, \\ \max(-\Delta\hat{\beta}_q, 0), & \beta_q = 0, \end{cases} \quad (13)$$

where

$$\Delta\hat{\beta}_q = \hat{\beta}_q|_{do(\alpha_p)} - \hat{\beta}_q|_{do(\neg\alpha_p)} = \hat{\beta}_q - \hat{\beta}_q|_{do(\neg\alpha_p)}, \quad (14)$$

we want the moving direction of affordance prediction after the intervention to be correct according to the GT affordance labels ( $\beta_q$ ). Concretely, for an instance with the labeled causal relation between  $[\alpha_p, \beta_q]$ , if the label  $\beta_q = 1$ , we expect the prediction change  $\Delta\hat{\beta}_q$  to be larger, indicating the elimination of  $\alpha_p$  leads to a drop of predicted probability. Because without the effect of  $\alpha_p$ , the probability of  $\beta_q$  should be **contrary** to the fact ( $\beta_q = 1$ ). Similarly, if  $\beta_q = 0$ , we expect  $\Delta\hat{\beta}_q$  to be smaller, i.e. the elimination of  $\alpha_p$  leads to an increase of predicted probability. The design of the ITE loss also follows the setting of this ITE score.

In  $\alpha$ - $\beta$ -ITE, the ITE score is multiplied by two factors of recognition performance:

$$\begin{aligned} P(\hat{\alpha}_p = \alpha_p) &= \begin{cases} \hat{\alpha}_p, & \alpha_p = 1, \\ 1 - \hat{\alpha}_p, & \alpha_p = 0, \end{cases} \\ P(\hat{\beta}_q = \beta_q) &= \begin{cases} \hat{\beta}_q, & \beta_q = 1, \\ 1 - \hat{\beta}_q, & \beta_q = 0. \end{cases} \end{aligned} \quad (15)$$

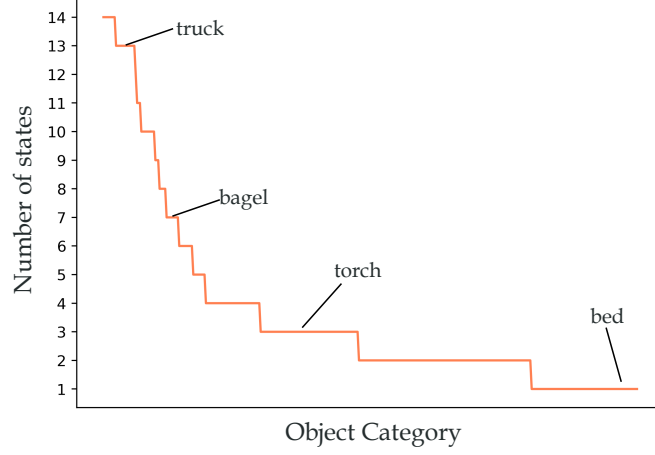


Figure 21: State distributions of different object categories.

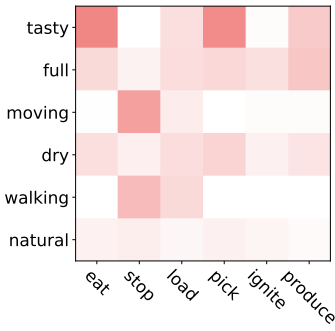


Figure 22: Attribute **conditioned** affordance matrix.



Figure 23: Attribute-affordance **correlation**.

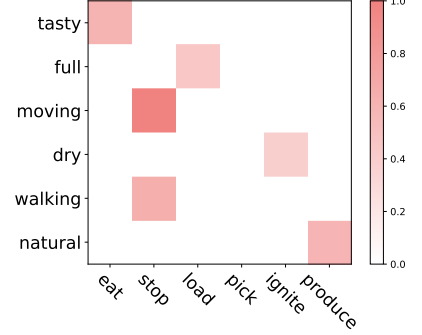


Figure 24: Attribute-affordance **causality**.

And the overall metric is:

$$\mathcal{S}_{\alpha-\beta\text{-ITE}} = \mathcal{S}_{\text{ITE}} P(\hat{\alpha}_p = \alpha_p) P(\hat{\beta}_q = \beta_q) \quad (16)$$

The factors measure the correctness of attributes and affordances. Hence a model achieves a high  $\mathcal{S}_{\alpha-\beta\text{-ITE}}$  only if it correctly predicts attribute and affordance and learns the causal relation between them.

In our experiments, for attribute/affordance recognition only, all methods adopt labels to learn knowledge from the data. In the evaluation of causal relation, only the “w/  $L_{\text{ITE}}$ ” models adopt the causal relation labels. We hope the models can automatically learn to mine and learn the intrinsic causalities. Thus, we design the ITE to evaluate this ability. Similar to our OCRN, some works [50, 75, 63] also try to marry supervised deep learning and causal inference.

## F. Baseline Details

We introduce the details of all baselines here:

**Fold I.** No arc between  $\alpha$  and  $\beta$ .

**(1) Direct Mapping from Visual Feature (DM-V):** feeding  $f_I$  into MLP-Sigmoids to predict  $P_\alpha, P_\beta$ . Each  $\alpha$  and  $\beta$  class owns customized MLP followed by Layer-Norm [76] to generate class-specific features and share the same MLP-Sigmoid in classification.

**(2) DM from Linguistic Representation (DM-L):** replacing the input representation  $f_I$  of DM-V with linguistic feature  $f_L$ , which is the expectation of Bert [64] of category names w.r.t  $P(O_i|I)$ .

**(3) Multi-Modality (MM):** mapping  $f_I$  to the semantic space via minimizing the distance to its  $f_L$ . The multi-modal aligned  $f_I$  is fed to an MLP-Sigmoids to predict  $P_\alpha, P_\beta$ .

**(4) Linguistic Correlation (LingCorr):** measuring the correlation between object and  $\alpha/\beta$  classes via their Bert [64] cosine similarity.  $P_\alpha, P_\beta$  are given by multiplying  $P(O|I)$  to correlation matrices.

**(5) Kernelized Probabilistic Matrix Factorization (KPMF) [65]:** calculating the Softmax normalized cosine similarity between each testing instance and all training

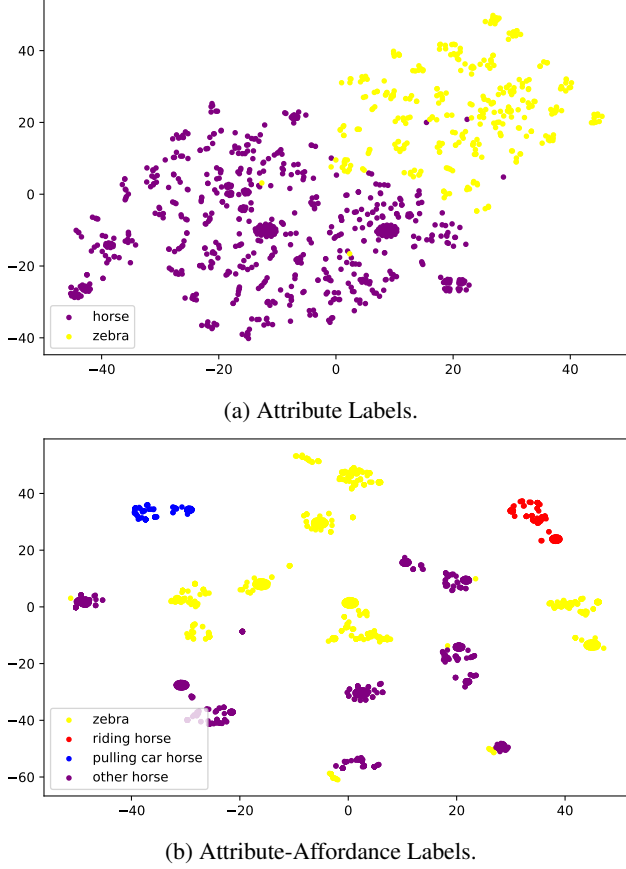


Figure 25: Clustering using attribute and attribute-affordance labels.

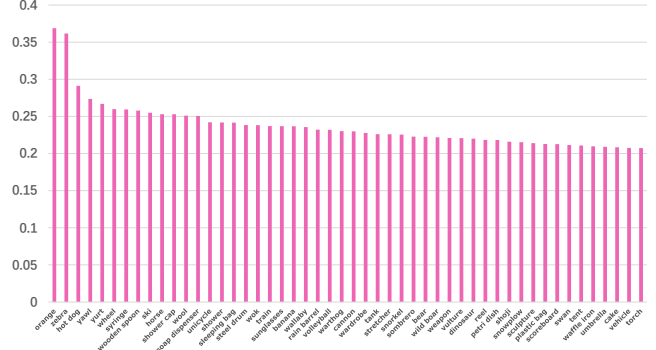
samples as weights. Then  $P_\alpha$  or  $P_\beta$  is generated as the weighted sum of GT  $\alpha$  or  $\beta$  of training samples.

**(6) A&B Lookup:** returning the expectation of category-level attribute or affordance vectors  $A_i, B_i$  w.r.t  $P(O_i|I)$ . In detail, seen category probabilities are obtained from GT prior  $M_A, M_B$ . Unseen category probabilities are voted by the top 3 most similar seen categories according to the cosine similarity of category Word2Vec [77] vectors. Then, we generate category-level attribute and affordance matrices  $M'_A, M'_B$  given the GT prior (seen) and similarity-based probabilities (unseen). Finally, we multiply  $P(O|I)$  with  $M'_A, M'_B$  to predict  $P_A, P_B$  and assign them to  $P_\alpha, P_\beta$  respectively.

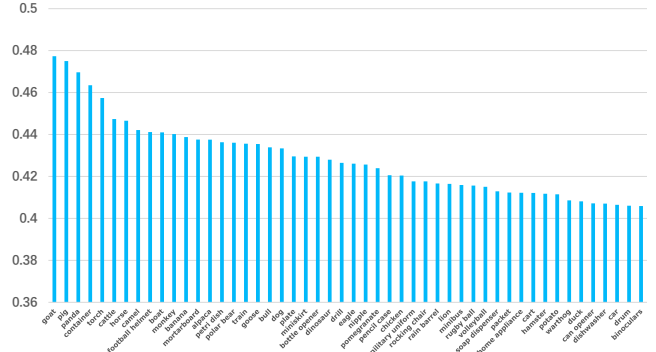
**(7) Hierarchical Mapping (HMa):** first mapping  $f_I$  to category-level attribute or affordance space by an MLP supervised by GT  $A$  or  $B$ . Then the mapped features are fed to an MLP-Sigmoids to predict  $P_\alpha$  or  $P_\beta$ .

**Fold II.** Directed arc from  $\beta$  to  $\alpha$ .

**(8) DM from  $\beta$  to  $\alpha$  ( $\text{DM-}\beta \rightarrow \alpha$ ):** training a  $\beta$  classifier with  $f_I$  same with DM-V, but using the concatenated representation of affordance as  $f_\beta$  to train the  $\alpha$  classifier.



(a) Difference between  $A$  and  $\alpha$  labels.



(b) Difference between  $B$  and  $\beta$  labels.

Figure 26: Top-50 object categories with the largest ratio of the difference between category- and instance-level labels.

**(9) DM from  $\beta$  and  $I$  to  $\alpha$  ( $\text{DM-}\beta I \rightarrow \alpha$ ):** training a  $\beta$  classifier with  $f_I$  same with DM-V, but using the concatenated representation of attributes  $f_\beta$  and objects  $f_I$  to train the  $\alpha$  classifier.

**Fold III.** Directed arc from  $\alpha$  to  $\beta$ .

**(10) DM from  $\alpha$  to  $\beta$  ( $\text{DM-}\alpha \rightarrow \beta$ ):** training an  $\alpha$  classifier with  $f_I$  same with DM-V, but using the concatenated representation of attributes as  $f_\alpha$  to train the  $\beta$  classifier.

**(11) DM from  $\alpha$  and  $I$  to  $\beta$  ( $\text{DM-}\alpha I \rightarrow \beta$ ):** training an  $\alpha$  classifier with  $f_I$  same with DM-V, but using the concatenated representation of attributes  $f_\alpha$  and objects  $f_I$  to train the  $\beta$  classifier.

**(12) Ngram [66]:** adopting Ngram to retrieve the relevance between  $\alpha$  and  $\beta$  and generating an association matrix  $M_{\alpha-\beta}$ . Then we multiply DM predicted  $P_\alpha$  with  $M_{\alpha-\beta}$  to estimate  $P_\beta$ .

**(13) Markov Logic Network (MLN-GT) [67]:** adopting MLN to model the  $\alpha - \beta$  relations following [16]. After training on OCL, we infer  $\beta$  with GT  $\alpha$  to estimate its *performance upper bound*.

**(14) Instantiation with attention (Attention):** feeding  $[f_\alpha, f_I]$  to an MLP-Sigmoid to generate attentions and predicting  $P_\beta$  by multiplying the attentions with  $P_B$ .





Figure 27: More OCL samples of object categories.

We operate baselines with a directed arc from  $\alpha$  to  $\beta$  (Fold III) to perform ITE. The ITE calculation needs **feature zero-masking** to eliminate the effect of specific attributes [63]. These methods (DM-At, DM-AtO, Attention, OCRN) follow the same ITE calculation (feature masking). Two unique cases are Ngram and MLN-GT. Ngram uses attribute probabilities to infer affordance. Thus, we randomize the specific attribute probabilities for Ngram to operate the ITE calculation. And MLN-GT must use GT attribute labels to distinguish the “positive” and “negative” causes and then reason out the effect affordance. Thus, in ITE, we directly eliminate its corresponding attribute input.

## G. Detailed Result Analysis

### G.1. Detailed Attribute and Affordance Performances

We compute and analyze the performance (AP) of OCRN on each attribute or affordance class in Fig. 34 and Fig. 35, which suggest that visually abstract concepts like *fake* are more difficult to model than concrete ones like *metal*, *breakable*. The performance of attribute classes is lower than affordance classes. This is mainly because the attributes have more diversity. Thus the *positive* instances of each attribute class are **less** than the affordance class.

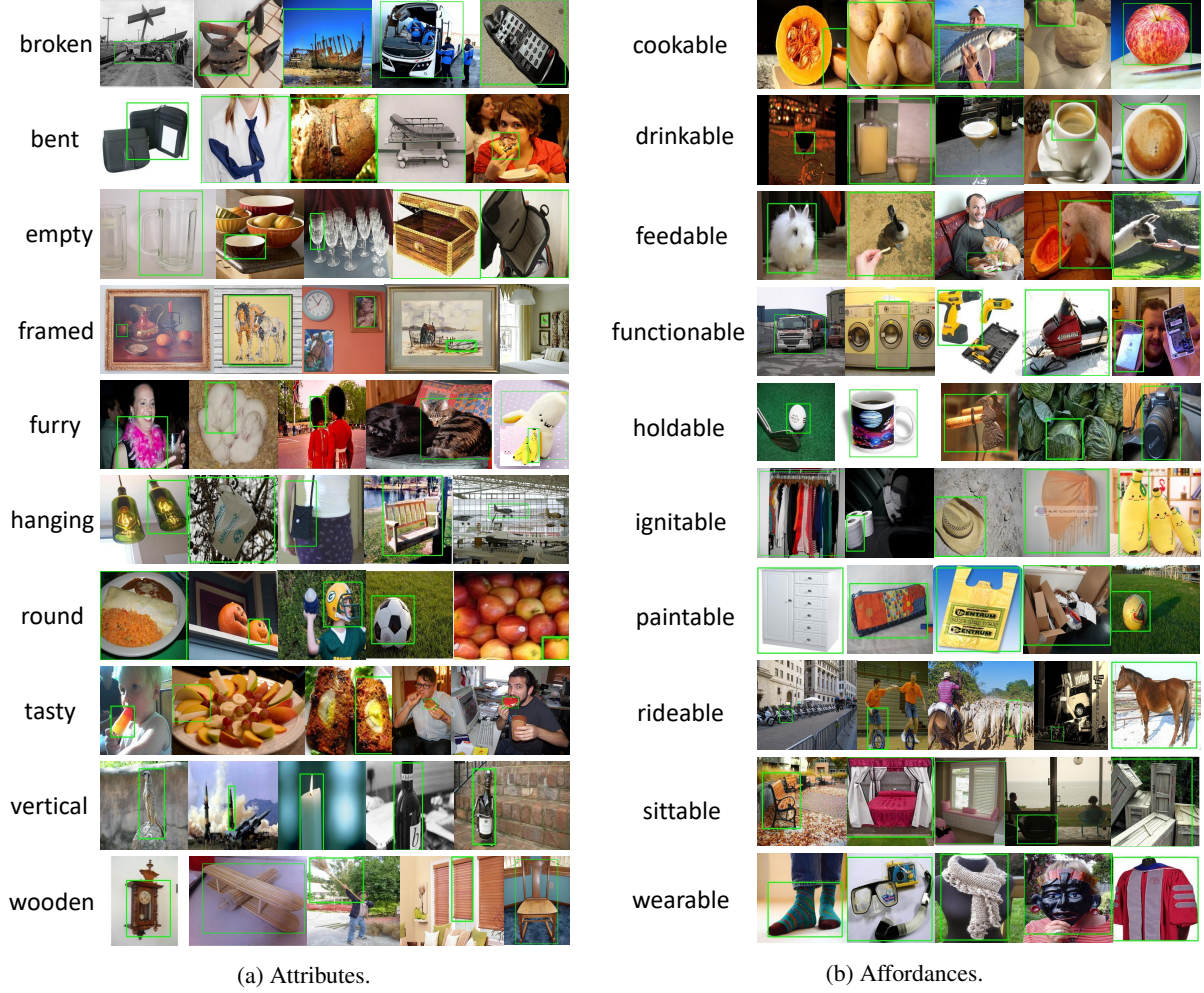


Figure 28: More OCL samples of attributes and affordances.

## G.2. Visualization of ITE Result

In Fig. 36, we show the correct instance proportions (%) of OCRN and Attention after ITE. (a) randomly chosen causal pairs  $[\alpha_p, \beta_q]$  with ground truth  $\beta_q = 1$ , expecting  $\hat{\beta}_q > \hat{\beta}_q|_{do(\alpha_p)}$ . (b) randomly chosen causal pairs  $[\alpha_p, \beta_q]$  with ground truth  $\beta_q = 0$ , expecting  $\hat{\beta}_q < \hat{\beta}_q|_{do(\alpha_p)}$ . The higher proportions indicate that OCRN performs better on ITE.

## G.3. Attribute and Affordance Recognition Given Detected Boxes

Though OCL is a high-level concept learning task with object boxes as inputs, we can also consider object detection in evaluation for practical applications. We adopt Swin Transformer (Swin) [68] as the detector. It is pretrained on COCO [2] and finetuned on the OCL train set with GT boxes of 381 categories. On the OCL test set, it achieves 22.9  $AP_{50}$  on object detection. Subsequently, it will pro-

vide detected box  $b_o$  for all models in inference. We can consider the detection effect in the attribute and affordance recognition metric to build a more strict criterion. Namely, all *false positive* detections (IoU<0.3 with referring to GT boxes) as the *false positives* of  $\alpha$  and  $\beta$  recognition too. Moreover, ITE calculation needs to construct the counterfactual of an object instance. If the inaccurately detected object box shifts according to the GT box, it is difficult to know whether the counterfactual comes from the attribute masking or visual content change, using the corresponding attribute-affordance causal relation labels of this GT box. Thus, considering the unique property of causal inference different from common recognition, here we do not report the ITE score. Tab. 5 shows the results given detected boxes. Due to the more strict criterion and detection quality, the performances of all methods degrade greatly. But OCRN still holds the superiority on two tracks.




Object States	Images	Attributes	Affordances
cat <i>caged/hold</i>		parked ✓ walking ✗ lit ✗	touch ✓ pull ✗ chase ✗
bus <i>toy</i>		fake ✓ rectangular ✗ moving ✗	drive ✗ lift ✓ load ✗
baked goods <i>raw</i>		tasty ✗ broken ✗ natural ✗	eat ✗ cook ✓ wash ✗
potato <i>mashed</i>		wet ✓ whole ✗ solid ✗	wash ✗ cook ✓ kick ✗
motorcycle <i>repairing</i>		metal ✓ parked ✓ moving ✗	drive ✗ check ✓ drag ✗

Figure 29: More OCL samples. We present objects in different states, together with their key attributes and affordances.






apple		fresh ✓	→	eat ✓
cattle		parked ✓	→	stop ✗
bird		dead ✗	→	feed ✓
pizza		heavy ✗	→	flip ✓
sheep		furry ✓	→	shear ✓

Figure 30: More OCL samples of causal relations.

#### G.4. OCL-Based Image Retrieval

We visualize the OCL reasoning performance by retrieving the top-score instances with OCRN. Some results are shown in Fig. 37 and Fig. 38. The model can correctly retrieve the related images, especially on some common concepts *e.g.*, *columnar*, *sit*.

#### H. Application on Human-Object Interaction (HOI) Detection

To further verify the generalization ability, we apply OCL to Human-Object Interaction (HOI) detection [78, 79, 53, 80] and help HOI methods boost their performances. HOI detection recently attracts a lot of attention and makes progresses [81, 82, 83, 84, 85, 86] thanks to the success of

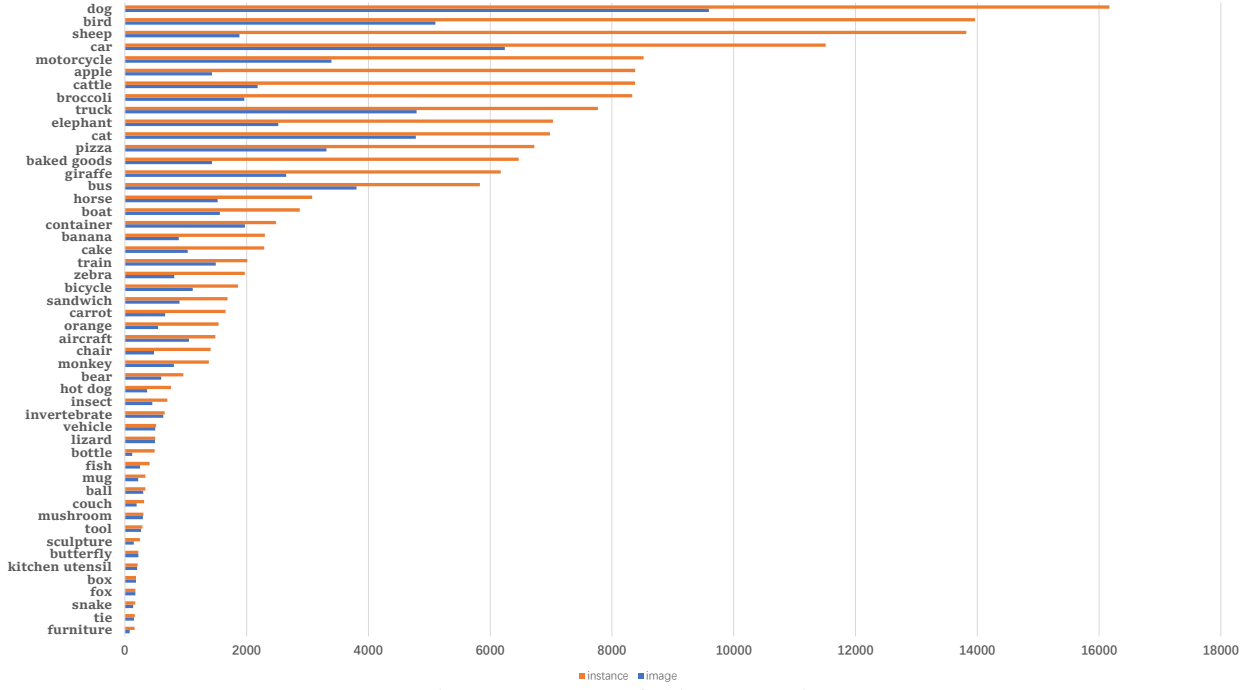


Figure 31: Counts of object categories.

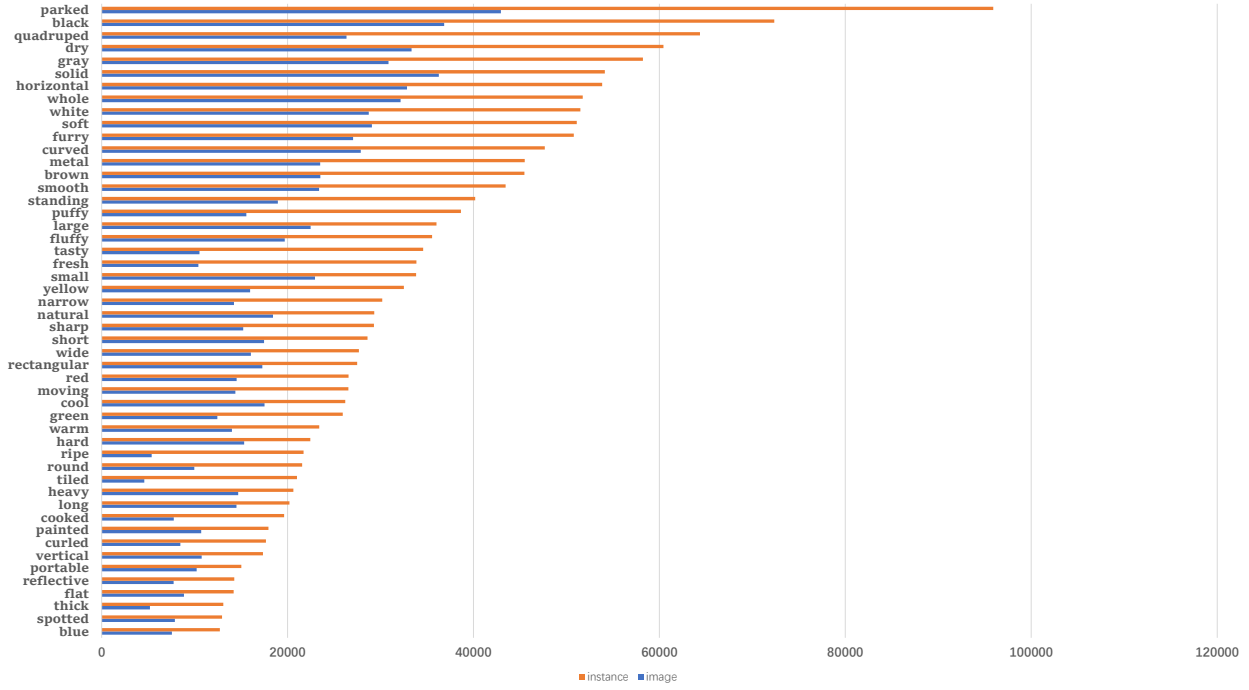


Figure 32: Counts of attribute classes.

deep learning and large-scale HOI datasets [53, 54, 87, 88].

HOI depicts the actions performed upon objects by humans. Usually, an object has multi-affordance, *i.e.*, a person can perform different actions upon it. But in an image, just one or several actions/affordances are usually happening/**activated**. Without object knowledge, previous meth-

ods [89, 90, 91] can find the activated affordances from hundreds of actions [53]. For example, for each human-object pair in HICO-DET [53], a model has to select one or several actions from the defined 116 actions. With OCL, things are different. OCL covers many actions, so we can use OCRN to infer  $P_\beta$  of an object to narrow the solution space. Thus,



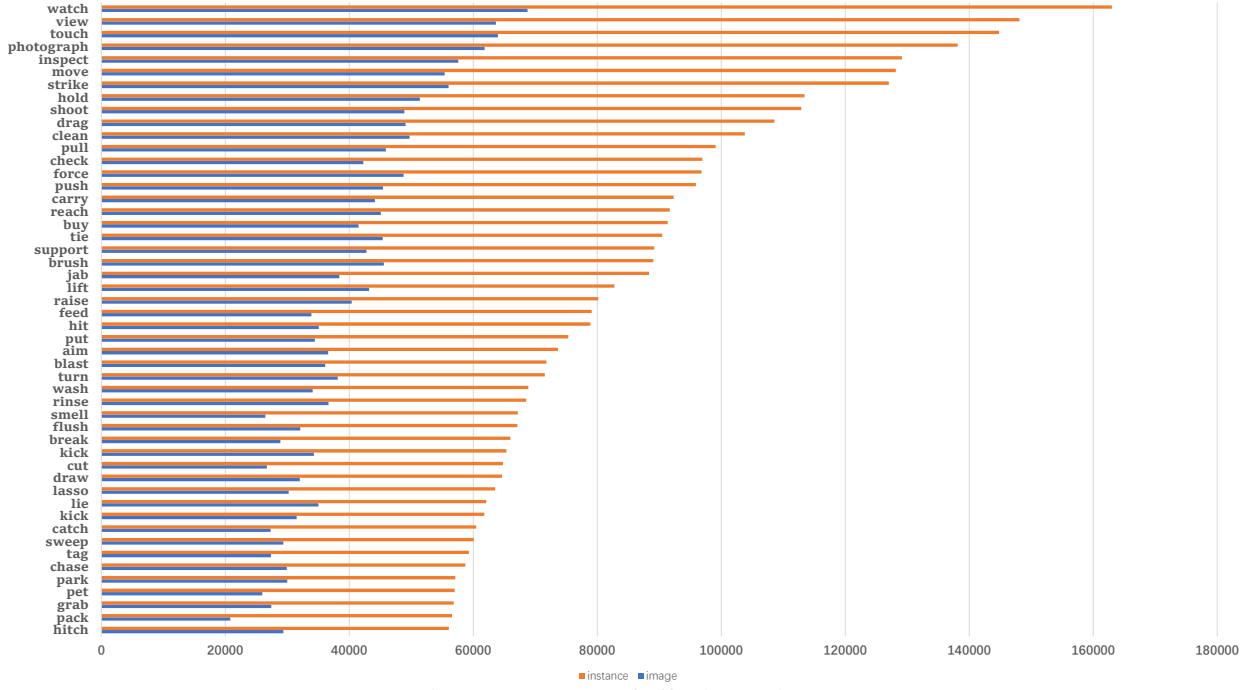


Figure 33: Counts of affordance classes.

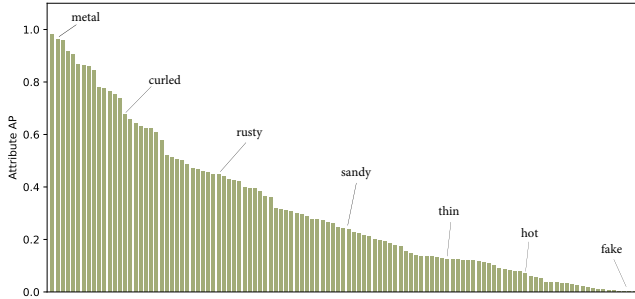


Figure 34: AP of attribute classes.

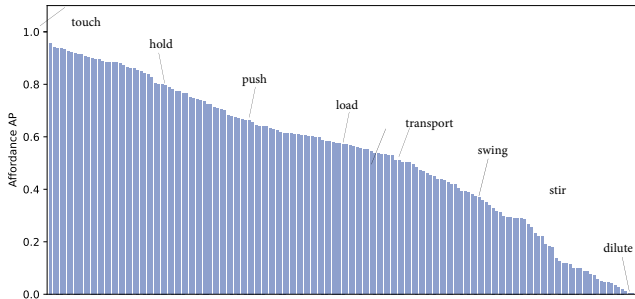


Figure 35: AP of affordance classes.

we propose two ways:

(1) **OCL Filtering:** We use  $P_\beta$  to narrow the action space with a threshold  $\gamma$  and generate  $P_\beta^\gamma$ . Affordances with probabilities higher than  $\gamma$  are kept and others are set to *zero* ( $\gamma = 0.5$ ). Then, the HOI model only needs to predict in

Method	$\alpha$	$\beta$
DM-V	7.4	11.0
DM-L	4.6	9.1
MM	5.4	9.9
LingCorr	1.7	5.6
KPMF	6.4	10.5
A&B-Lookup	4.1	5.8
HMa	6.5	10.9
DM-At	6.8	10.5
DM-AtO	6.6	10.8
Ngram	5.1	10.2
MLN-GT	-	-
Attention	5.5	10.1
OCRN	<b>7.9</b>	<b>11.3</b>

Table 5: Attribute and affordance recognition results given detected boxes from Swin Transformer [68].

a narrowed action space. In practice, we multiply the prediction  $P_{HOI}$  from HOI model with  $P_\beta^\gamma$  element-wisely to obtain the final prediction  $P'_{HOI} = P_{HOI} * P_\beta^\gamma$ .

(2) **Human-as-Probe:** Another more straightforward way is to predict HOI via OCL directly. We treat the human paired with the object as a **probe**. Assuming the human feature is  $f_h$  and human-object spatial configuration feature is  $f_{sp}$  (from [89, 90]). As  $P_\beta$  indicates all possible affordances, the ongoing actions can be seen as the **instantiation** of  $P_\beta$ , i.e., they are activated by the “probe”  $f_h$  and  $f_{sp}$ . So we use  $f_h$  and  $f_{sp}$  to generate attention  $A_{h+sp}$  via

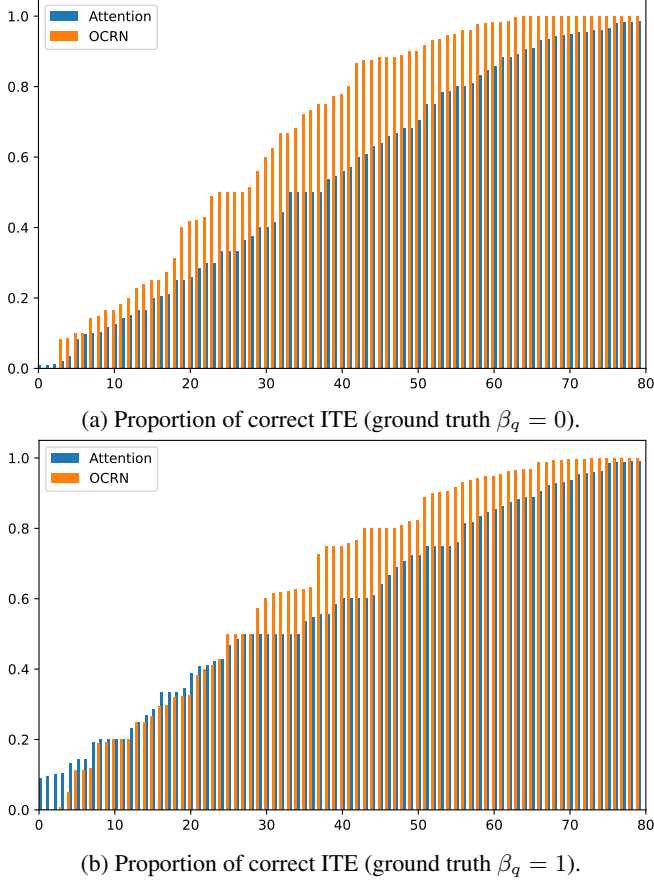


Figure 36: ITE given different  $[\alpha_p, \beta_q]$ .

MLP-Sigmoid. Then we operate  $P_\beta * A_{h+sp}$  and late fusion to get the final prediction  $P'_{HOI} = (P_\beta * A_{h+sp} + P_{HOI})/2$ .

Concretely, we use OCRN to enhance HOI detection models (iCAN [90], TIN [89], IDN [91]) on HICO-DET [53]. As OCL merely contains 15 object categories in HICO-DET [53], the rest 65 object categories are **unseen**. We embed OCRN into three HOI models according to OCL filtering and Human-as-Probe, and the public model checkpoints of [90, 89, 91] are used.

The results are shown in Tab. 6. With OCL filtering, iCAN [90], TIN [89], and IDN [91] achieve a gain of mAP by 0.65%, 0.90%, and 0.77% respectively. The Human-as-Probe is more suitable for HOI detection and contributes a performance boost of 1.50%, 1.46%, and 0.98% to three models. These strongly verify the efficacy and generalization ability of OCL.

## I. Comparison on Debiasing

The motivation of the OCRN is to follow the prior knowledge of the three levels of objects with a deep learning-based causal graph model, to pursue the object un-

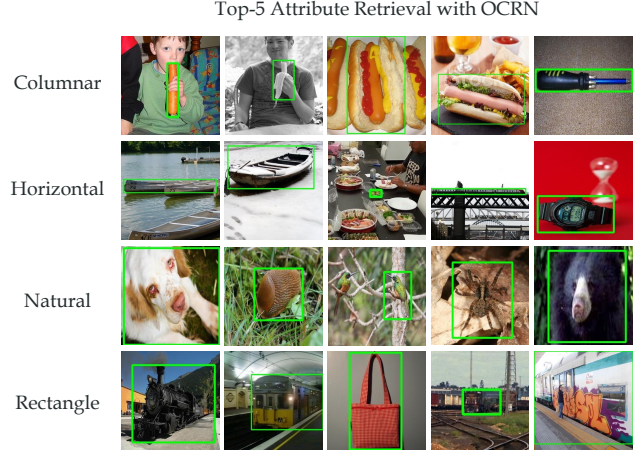


Figure 37: Top-5 attribute retrievals on the OCL test set.

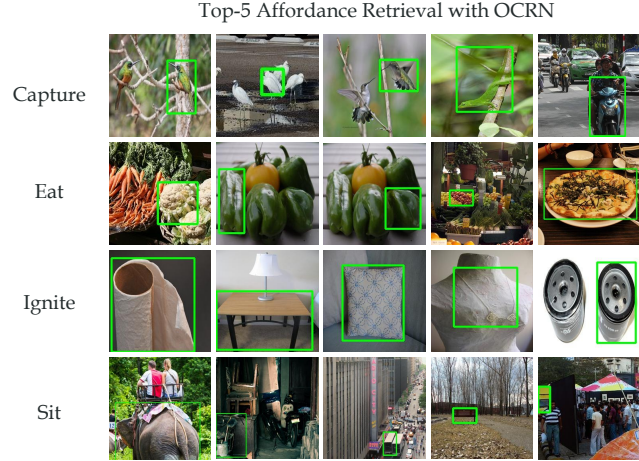


Figure 38: Top-5 affordance retrievals on the OCL test set.

Method	Full	Rare	Non-Rare
iCAN	14.84	10.45	16.15
iCAN+Filtering	15.49	8.76	17.50
iCAN+Probe	<b>16.34</b>	<b>11.66</b>	<b>17.74</b>
TIN	17.03	13.42	18.11
TIN+Filtering	17.93	13.79	19.17
TIN+Probe	<b>18.49</b>	<b>15.02</b>	<b>19.58</b>
IDN	23.36	22.47	23.63
IDN+Filtering	24.13	23.74	24.24
IDN+Probe	<b>24.34</b>	<b>24.03</b>	<b>24.43</b>

Table 6: Results of HOI detection (using detected object boxes).

derstanding beyond the common direct mapping from pixels to labels, and to avoid the bias estimation such as in the **Simpson's paradox** [20]. Thus, we use intervention to deconfound the confounder *category* and exclusive the pos-



Figure 39: Attribute bias (w/ and w/o deconfounding) for category frying pan.

Model	Test Inference	$\alpha$ Amp.	$\beta$ Amp.
OCRN	$\arg\max_y P(y x)$	<b>0.127</b>	<b>0.112</b>
DM-V + Joint ND-way Softmax	$\arg\max_y \max_d P_{te}(y, d x)$	0.151	0.158
DM-V + Joint ND-way Softmax	$\arg\max_y \sum_d P_{te}(y, d x)$	0.148	0.154
DM-V + N-way classifier per domain	$\arg\max_y P_{te}(y d^*, x)$	0.135	<b>0.112</b>
DM-V + N-way classifier per domain	$\arg\max_y \sum_d s(y, d, x)$	0.147	0.145

Table 7: Comparison with debiasing models.

sible spurious bias and correlation imported bias from imbalanced object categories. Overall, we propose our OCRN in a causal inference perspective instead of the pure classification viewpoint, which also suits our causal graphical model well. Similar cases are also proposed in recent works like [50, 75, 63]. Moreover, to better compare our method with the common debiasing methods, we further conduct the experiments as follows.

We regard  $\alpha, \beta$  recognition as multiple independent binary classification tasks and implement some methods introduced in [92] on our strong baseline DM-V to reduce bias from object categories. We use **mean bias amplification (Amp)** in [93] as bias evaluation metric: small Amp means model suffers less from data category bias. The test results are shown in Tab. 7. The proposed OCRN has comparable or smaller bias amplification than the variants of DM-V since our model follows the causal graph and exploits the tools of causal inference, while most methods for category bias are from the view of classification.

To verify the debiasing of OCRN, we compare the model bias of OCRN **w/ or w/o deconfounding**. The bias of category  $O$  upon an attribute  $\alpha$  is measured following [93], by  $b(O, \alpha) = c(O, \alpha) / \sum_{\alpha'} c(O, \alpha')$ . When measuring **data** bias,  $c(O, \alpha)$  is the number of co-occurrence of  $O$  and  $\alpha$  in OCL, and when it comes to **model** bias,  $c(O, \alpha)$  is the sum of probabilities that  $O$  are predicted positive with  $\alpha$ . The bias of  $\beta$  is measured in the same manner. Fig. 39 and 40 show some examples of the biases of training data and models, indicating that OCRN deconfounding effectively pre-

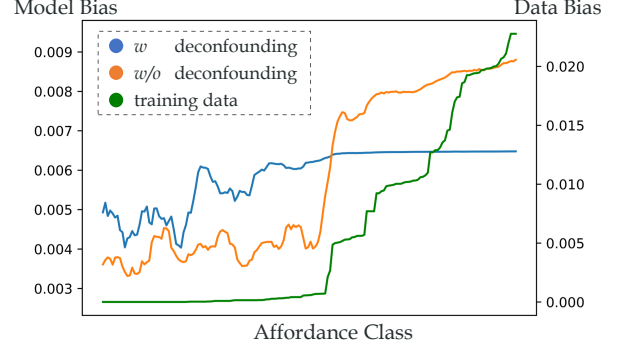


Figure 40: Affordance bias (w/ and w/o deconfounding) for category giraffe.

vents the model from bias toward the train set.

## J. Discussion about States

We did not use object states in our model because there is also a **compositional zero-shot problem** and object-state pairs, *i.e.*, there can be **unseen** states in real-world data. Differently, affordances are more general. The models explicitly incorporating object states will fail to generalize to these zero-shot states and it adds to the object category bias. In experiments, the state supervision during training would indeed *slightly improve* the affordance recognition performance, since instances in the **same state** lie in a tight cluster in affordance label space. But this will hurt the ITE performance greatly.

## K. Discussion about Causality and Causal Graph

Annotating causality in the real world is extremely difficult. In data annotation, we have met numerous ambiguities and difficulties to confirm the “right” causal relations. To address these challenges, we follow the following principles: (1) Firstly, we only emphasize **clear** and **strong** causal relations via crowdsourcing, but omit the vague ones. (2) Second, we take an object **affordance-centric** viewpoint to look at the possible causal relations. (3) We would rather **discard** than condone the controversial situation in the annotation. (4) We only focus on the simple relations between **one** attribute and **one** affordance, instead of the very complex compositions of multiple attributes and affordances which are almost impossible to annotate. Therefore, we finally find that we can label a **very small percentage** of all arcs with the whole causal graph consisting of so many nodes (category, attributes, affordances, contexts, etc.) while keeping the quality.

Our causal graph follows the human priors from our experts and crowdsourcing annotators. Some previous works

also follow this before designing the method, such as [16]. From the viewpoint of causal discovery [20, 75, 63, 50], the above arcs (*e.g.*, the inverted arc from attribute to category in the causal graph directed acyclic graph, DAG) are indeed possible. However, here, we mainly study the object concept learning problem, especially attribute and affordance learning for intelligent robots and embodied AI. Thus, from the perspective of affordance learning, we think the arcs from category to attribute and affordance is more vital and meaningful to us.

Causality can also be confused with **enabling condition**. In OCL, the affordance of an object indicates what human *can do* to/with it. In this case, “fresh” causes “**eat-able**” (**rather than causes “eat” action**). As causality is discussed in the view of **embodied agents**, this rule can hold. In modern causal inference models like structured causal models (SCM), causality and enabling conditions are not strictly distinguished. As stated by Cheng *et al.* [94], causes and enabling conditions hold the same logical relation to the effect in those terms and the methods that explain their distinction come from the subject judgment of humans. The distinction can be explained based on the *normality* of potential factors, or considering the existing assumption of the inquirer. They proposed an approach by measuring the covariation between potential factors to the effect over a set of questions. So in SCM, both will be represented as nodes and involved in causal mechanisms. OCL follows the “open” setting: affordance is a subjective property of the object, so all reasons given by humans/robots (including enabling conditions) are regarded as causal factors.